Circuits and Systems
Mekelweg 4,
2628 CD Delft
The Netherlands
http://ens.ewi.tudelft.nl/

PHILIPS
sense and simplicity

M.Sc. Thesis

Illumination control of an LED lighting system based on localized occupancy

David Caicedo

Abstract

Light emitting diode (LED) based systems are considered to be the future of lighting. We consider the problem of energy-efficient illumination control of such systems. Energy-efficient system design is based on two aspects: localized information of occupancy and optimization of dimming levels of the LEDs. Specifically, we are interested in minimizing the power consumption of an LED system, subject to providing uniform illumination at a pre-specified level around occupied zones, by determining the dimming levels of the LEDs. Localized occupancy information (i.e. occupied zones) is determined by an ultrasonic array sensor while providing a natural interface for illumination control. We present algorithms for localizing and tracking an occupant in an indoor environment. We show that the optimization problem for illumination can be solved by linear programming and use the simplex algorithm to determine the dimming levels. The efficacy of the system is evaluated with numerical simulations and experimental data.

TU Delft

Illumination control of an LED lighting system based on localized occupancy

Thesis

submitted in partial fulfillment of the
requirements for the degree of

Master of Science

in

Electrical Engineering

by

David Caicedo
born in Guayaquil, Ecuador

This work was performed in:

Distributed Sensor Systems Group
Philips Research Europe
High Tech Campus
5656 AE Eindhoven, The Netherlands

Delft University of Technology

Delft University of Technology
Department of
Telecommunications

The undersigned hereby certify that they have read and recommend to the Faculty of Electrical Engineering, Mathematics and Computer Science for acceptance a thesis entitled **"Illumination control of an LED lighting system based on localized occupancy"** by **David Caicedo** in partial fulfillment of the requirements for the degree of **Master of Science**.

Dated: June 7, 2010

Chairman:

Prof. dr. ir. Alle-Jan Van der Veen, CAS, TU Delft

Advisors:

Dr. ir. Ashish Pandharipande, Philips Research Europe

Dr. ir. Geert Leus, CAS, TU Delft

Committee Members:

Prof. dr. ir. Urbashi Mitra, University of Southern California, USA

Abstract

Light emitting diode (LED) based systems are considered to be the future of lighting. We consider the problem of energy-efficient illumination control of such systems. Energy-efficient system design is based on two aspects: localized information of occupancy and optimization of dimming levels of the LEDs. Specifically, we are interested in minimizing the power consumption of an LED system, subject to providing uniform illumination at a pre-specified level around occupied zones, by determining the dimming levels of the LEDs. Localized occupancy information (i.e. occupied zones) is determined by an ultrasonic array sensor while providing a natural interface for illumination control. We present algorithms for localizing and tracking an occupant in an indoor environment. We show that the optimization problem for illumination can be solved by linear programming and use the simplex algorithm to determine the dimming levels. The efficacy of the system is evaluated with numerical simulations and experimental data.

Acknowledgments

This thesis would not have been possible without the help and contribution of a number of people, to whom I would like to express my sincere gratitude. I am heartfelt thankful to my advisors Dr. Ashish Pandharipande and Dr. Geert Leus for their supervision, guidance and encouragement.

I would like to thank also to the Philips Research laboratory staff, in particular, to my office mates: Ton Hellings, Alberto Caballero, Diego Benavente, Andreas Achtzehn, Stuart De Haan and Maarten Brugmans. Thanks to all the intern community, as well, especially to Henry Haus, Clémentine Javaux, Tania Garcia, Pasquale Coirazza, Eva Abal, Deniz Atli, Jérôme Perrin and Guillermo Fernández-Blanco for making my stay in Eindhoven more pleasant.

Further thanks should also go to my colleagues in Delft for their support and friendship, mainly to Victor Vélez, José Luis Almodóvar, Maxim Volkov and Aarabi Kumar. Last but not least, I would like to thank my family for their love and support during all this time. Special thanks to my aunt, Narcisa, and her family for their support and company here in The Netherlands.

David Caicedo
Delft, The Netherlands
June 7, 2010

Contents

List of Figures

List of Tables

1 Introduction

Energy efficiency is one of the design drivers in smart lighting systems and more generally in green buildings. The study in [1] for instance shows that office lighting accounts for almost 20% of the overall energy consumption. Occupancy-based illumination control of lighting systems is one way to realize savings in energy. In its simplest form, occupancy information is used to control an entire lighting system in a room to provide illumination only when the room is determined to be occupied. The presence of occupants is determined by simple motion detectors e.g., passive infrared sensor, ultrasound.

More advanced control solutions to illuminate lighting systems are provided by using enhanced occupancy information. By enhanced occupancy information, we refer to information regarding location of occupants, their movement trajectories in addition to simple determination of whether a room is occupied. An example of such illumination control solution is to provide selectively uniform illumination levels at a desired level around occupied zones and at lower levels in other areas.

Those advanced control solutions require tunable and energy-efficient illumination systems. Light emitting diodes (LEDs) are set to become the next generation source of these illumination systems. They offer longer life times, dynamic light effects and greater design flexibility. Flexibility in tuning LEDs in particular means that the design of LED based systems offers greater potential for energy savings and illumination rendering [2], [3], [4].

1.1 Problem statement

We consider the problem of energy-efficient illumination control of an LED lighting system based on localized occupancy information. This system is considered in a typical workplace setting of an office room with one or more occupants.

Furthermore, we look at two aspects of the problem. One aspect is to estimate which zones are occupied in the office room (i.e. locations of the occupants). The second aspect is to provide uniform illumination levels at a desired level (at an illumination level required as per workspace norms) around those occupied zones and at lower levels in other areas in the office room while minimizing the total power consumption of the LED lighting system.

1.2 Related work

Different indoor localization and navigation solutions have been proposed in past literature. Similarly, several aspects of LED lighting system design have been considered in the past. In this section, the most relevant works for the thesis are reviewed.

Solutions for indoor localization and navigation include the works in [5]-[10]. These solutions cannot be easily interfaced with a lighting system and hence are impractical for lighting control. Furthermore, they require that the user carries some sensor or tag at all times which is intrusive. Control of lighting is then also dependent on whether users carry the tag. Additionally, a communication interface is required between the tag and the lighting system. In contrast to these approaches, we provide a single sensor solution to determine enhanced occupancy information for indoor environments (e.g., offices), while providing a natural interface to lighting and building systems. The proposed method does not require that the user carries a sensor or tag (i.e. any user can be located) and hence can be easily integrated with the illumination control system.

Continuous Wave Doppler radars described in [11] are not a natural choice for indoor environments due to propagation issues. Electromagnetic waves travel through walls separating adjacent rooms. On the other hand, ultrasound waves do not travel through solid objects (e.g. walls) and so the coverage of an ultrasound based sensor can be limited to a specific area. Hence, we proposed an ultrasonic sensor array for indoor localization in an office room.

A framework for the design of lighting systems based on daylight control and occupancy information was developed in [12]. The approach used there considered the maximization of occupant utility functions taking energy efficiency into consideration. Further, in solving for the illumination levels, the light sources were assumed to have narrow beams. On the contrary, we are particularly interested in energy-efficient illumination control of an LED lighting system. Furthermore, we consider LEDs with broader beams.

1.3 Thesis goal

The major goal of the thesis is to design an illumination control system for an office room based on localized occupancy information.

In particular, we consider algorithms to obtain enhanced occupancy information using an ultrasound based sensor. Moreover, the proposed solution is implemented in the test lab in order to obtain experimental results and evaluate its performance.

Additionally, we solve the problem of illumination control under the constraints of providing uniform illumination and minimizing the total power consumption of the LED lighting system. Numerical simulations are performed to evaluate the performance of the proposed illumination control algorithm of the LED lighting system.

1.4 Thesis organization

The thesis is organized as follows. In Chapter 2, a framework for obtaining enhanced occupancy information is established. High accuracy localization information is provided using a single ultrasound based sensor array solution. Later, Chapter 3 presents the illumination control solution. The problem is shown to belong to the family of linear programming problems and the simplex method is used to obtain the optimal solution. Results of this Chapter have been reported in the journal of Lighting Re-

search and Technology [13]. Results of the ultrasonic sensor array solution based on pre-defined experiments are shown in Chapter 4. These results are further evaluated with simulations for the illumination control algorithm. Finally, conclusions drawn from the results and further work which can improve the system performance are given in Chapter 5.

Notation

Given 2 coordinates (x_1, y_1) and (x_2, y_2), the distance between them, or the 2-norm of the difference between the coordinates is given by $||\,(x_2, y_2) - (x_1, y_1)\,||_2 = \sqrt{(x_2 - x_1)^2 + (y_2 - y_2)^2}$. For a real value x, its absolute value will be written as $|x|$ and its floor by $\lfloor x \rfloor$. For two positive numbers a and b, the remainder of division of a by b is given by the modulo operation, written as $a \mod b$.

Localized Occupancy Estimation

2

In this chapter, we propose an indoor localization method based on an ultrasonic sensor array solution. This sensor array solution comprises of a single ultrasound based transmitter and a co-located linear array of M receivers as depicted in Fig. 2.1. A short duration sinusoidal wave is transmitted at a regular repetition interval. The reflections of moving targets are used for further processing. By using the time of flight and the direction of arrival (DoA) of these signals, we obtain a 2-D localization of the occupant in the room. The accuracy of this localization is further improved by implementing a tracking algorithm based on a movement model of the occupant. Multipath is mitigated by using a simple criterion: multipath may result in infeasible locations and hence those infeasible locations are discarded.

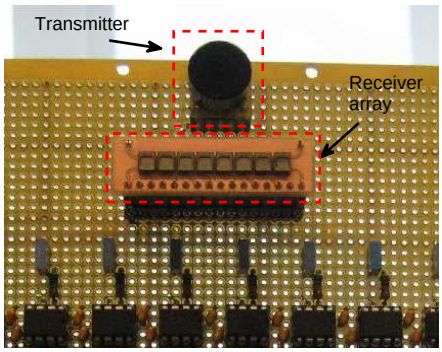

Figure 2.1: Ultrasound sensor array solution

2.1 Ultrasonic sensor array solution

We consider a sensor array solution located in a room of length l and width w. Furthermore, we assume that the sensor array is located at the middle of the room's width and at a height $\hat{h}$ as shown in Fig. 2.2. We assume a coordinate system with the origin at the center of the room as shown in Fig. 2.3. We will not introduce a z-coordinate as it is not required. The receiver array is spaced along the y-axis with separation Δm amongst adjacent receivers as shown in Fig. 2.4. This separation is given by

$$\Delta m = \frac{\lambda}{2}$$

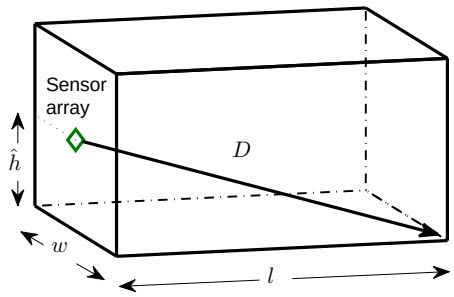

Figure 2.2: Dimensions of the room

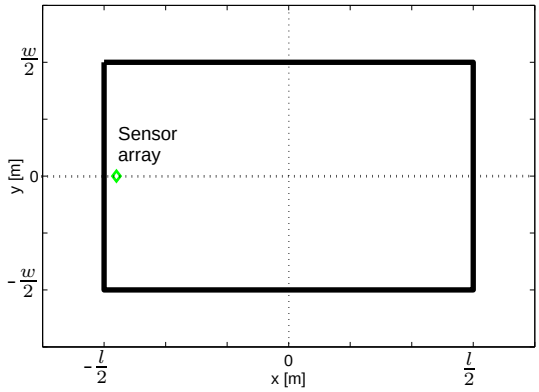

Figure 2.3: Coordinate system for the room

and hence no granting lobes are observed in the scanning range. The transmitter and receivers are assumed to be omnidirectional[1].

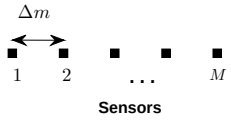

Figure 2.4: Receiver array configuration

The targets are assumed to be located in the far field of the sensors. Hence, the phase shift of the received signal between sensors depends only on the DoA of the signal

[1]Practical beamwidth limitations are discussed in Section 4.1.

and configuration of the sensors. The far field approximation in practice is valid for our application as is shown further in Appendix A.1.

Thus, the phase shift, ϕ_m, of the received signal by the mth sensor with respect to the first sensor is given by

$$\phi_m(\theta) = 2\pi(m-1)\Delta m \sin(\theta). \tag{2.1}$$

Accordingly, we can steer the receiver's beam in the direction θ by using the array response vector $\boldsymbol{a}(\theta)$ given by

$$\boldsymbol{a}(\theta) = \begin{bmatrix} 1 \\ e^{2\pi j \frac{\Delta m}{\lambda}\sin(\theta)} \\ e^{2\pi j 2\frac{\Delta m}{\lambda}\sin(\theta)} \\ \vdots \\ e^{2\pi j (M-1)\frac{\Delta m}{\lambda}\sin(\theta)} \end{bmatrix}. \tag{2.2}$$

2.2 Practical design considerations

Ultrasonic refers to high frequency sound waves (frequency range above 20 kHz), which are inaudible to human beings. In our system, a transducer[2] with central frequency $f_c = 40$ kHz is used. Let $v_s = 344$ ms^{-1} be the speed of sound in air. The wavelength, λ, for a 40 kHz sound signal is given by

$$\begin{aligned} \lambda &= \frac{v_s}{f_c} \\ &= \frac{344}{40000} \\ &= 8.6 \text{ mm}. \end{aligned}$$

Let the length and width of the room be respectively $l = 4.5$ m and $w = 3$ m (e.g. a typical office room). Furthermore, we assume that the sensor array is located at a height $\hat{h} = 1.2$ m. This height is typically above various objects such as furniture and equipments in an office room.

Let us define a maximum coverage range D for the system,

$$\begin{aligned} D &= \sqrt{l^2 + (0.5w)^2 + \hat{h}^2} \\ &\approx 5 \text{ m}. \end{aligned} \tag{2.3}$$

This limit assures an unambiguous range detection of targets within the room. Any object with a distance D' longer than D (e.g. multipath) is detected at a closer range, at a distance $D' \mod D$.

[2] A transducer is a device that converts one type of energy (pressure wave) into another (electrical signal).

This maximum range, D, corresponds to a round-trip time, RT, from the sensor to the object equal to

$$\begin{aligned} RT &= 2\frac{D}{v_s} \\ &= 2\frac{5}{344} \\ &\approx 30 \text{ ms.} \end{aligned} \tag{2.4}$$

2.2.1 Indoor environment

An indoor environment presents some difficulties. The presence of different objects and structures (e.g. desk, walls) close to the intended target (occupant) increases the number of unwanted echoes (clutter) and multiple reflections of the intended echo (multipath).

Clutter is the term used for reference signals coming from unwanted targets. These unwanted targets are divided mostly into stationary and moving clutter. The stationary clutter originates from walls, desk and other objects and structures located in the room. On the other hand, moving clutter is produced by the wind moving a curtain or a plant.

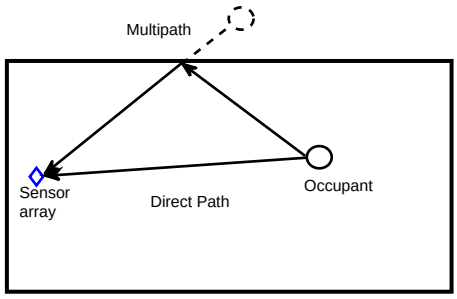

Figure 2.5: Multipath scenario

Multipath refers to the multiple reflections of the intended signal by nearby structures. A multipath scenario is depicted in Fig. 2.5. The location of the multipath usually lies outside the limits of the room. Hence, we can use this idea to recognize a multipath as explained later in Subsection 2.3.5.

2.2.2 Considerations for the speed of the occupant

The movement of the occupant introduces a shift in frequency on the received echo known as the Doppler effect. In a monostatic system[3], the Doppler shift $\hat{f}$ is given by

$$\hat{f} = -2\frac{v_r}{v_s} f_c$$

[3]In a monostatic system, the transmitter and receiver are located at the same position.

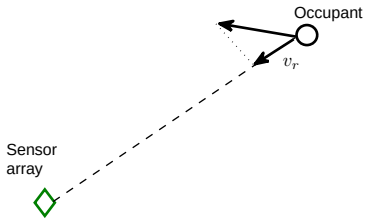

Figure 2.6: Radial speed of a moving occupant with respect to the sensor array

where v_r is the radial speed of the occupant with respect to the sensor array as shown in Fig. 2.6.

In practice, occupants in an office room do not move with high speed. Thus, we consider a maximum radial speed of $v_{max} = 4$ ms^{-1} for our system (i.e. the system can only detect occupants moving slower than this limit). This upper limit corresponds to a maximum Doppler frequency given by

$$\begin{aligned} \hat{f}_{max} &= 2\frac{v_{max}}{v_s} f_c \\ &= 2\frac{4}{344}40000 \\ &\approx 1000 \text{ Hz.} \end{aligned} \tag{2.5}$$

2.2.3 Transmitted waveform

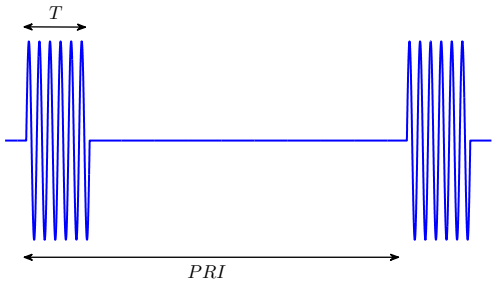

Figure 2.7: Short duration pulse

A sequence of sinusoidal pulses of duration T is transmitted at a regular interval of time PRI (pulse repetition interval) as depicted in Fig. 2.7. Let the transmitted pulse be given by

$$s(t) = \Pi\left(\frac{t}{T}\right) e^{j2\pi f_c t}$$

with

$$\Pi(t) = \begin{cases} 1 & \text{if } 0 \leq t \leq 1 \\ 0 & \text{otherwise.} \end{cases}$$

By determining the elapsed time τ from transmission until reception of the echo, the range d is estimated by

$$d = \frac{\tau}{2} v_s.$$

We choose a range resolution $\Delta D = 0.344$ m, which corresponds to a duration T equal to

$$\begin{aligned} T &= 2\frac{\Delta D}{v_s} \\ &= 2\frac{0.344}{344} \\ &= 2 \text{ ms.} \end{aligned} \tag{2.6}$$

This is the minimum separation in range between two people that the system can resolve.

The parameter PRI depends on the maximum round-trip time, RT, and the pulse duration, T, given by (2.4) and (2.6), respectively, and is equal to

$$PRI = RT + T = 32 \text{ ms.}$$

The received signal at the mth sensor during the interval PRI can now be written as

$$\begin{aligned} u_m(t) &= \sum_{k=1}^{K} \beta_k(t)\, \Pi\left(\frac{t-\tau_k(t)}{T}\right) e^{2\pi j f_c t + j\phi_{m,k}} + \\ &\quad \sum_{z=1}^{Z} \beta_z(t)\, \Pi\left(\frac{t-\tau_z(t)}{T}\right) e^{2\pi j\left(f_c + \hat{f}_z(t)\right)t + j\phi_{m,z}(t)} + \\ &\quad n_m(t) \end{aligned} \tag{2.7}$$

where β_i and τ_i are respectively the complex attenuation factor and delay of the ith echo denoted by

$$\begin{aligned} \beta_i(t) &= b_i e^{j2\pi \frac{2d_i(t)}{\lambda}} \text{ and} \\ \tau_i(t) &= 2\frac{d_i(t)}{v_s}. \end{aligned}$$

Here, n_m is additive white Gaussian noise at the mth sensor. K and Z are the number of echoes coming from non-moving objects and moving objects, respectively. $\hat{f}_z(t)$ is the Doppler frequency of the zth moving object given by (2.5) and $\phi_{m,i}$ is the phase at the mth sensor of the ith echo given by (2.1).

2.2.4 Discretization of locations

In our application, we need to discretize the location of the occupant. A high granularity for the discretization provides high accuracy[4] but a large set of locations. We need to

[4]The accuracy of the sensor depends on the closeness between the measured and the real location.

analyze each location from the set and so the processing time is large. Hence, there is a trade off between the processing time and the accuracy of the system.

We choose an accuracy for the system of $\frac{\Delta D}{2}$ (half of the range resolution), so the number of locations is limited. Accordingly, the discrete values for range are given by

$$d(\rho) = (\rho - 1)\frac{\Delta D}{2};\ \rho = 1, 2, \ldots, \left\lfloor \frac{2D}{\Delta D} \right\rfloor \tag{2.8}$$

and for DoA

$$\theta(\varsigma) = \varsigma \Delta DoA - 90;\ \varsigma = 0, 1, \ldots, \left\lfloor \frac{180}{\Delta DoA} \right\rfloor \tag{2.9}$$

where

$$\Delta DoA \approx \tan^{-1}\left(\frac{\Delta D}{2 \times 5}\right) \approx 2 \text{ degrees.}$$

2.3 Occupant localization and tracking system

The following approach for detecting and localizing an occupant is used. First, we filter out the signal coming from the background (e.g. furniture). Then, we estimate the location of the moving targets (range and DoA). Next, we improve the accuracy of the locations by tracking the targets. Finally, we discard the locations that correspond to multipath.

2.3.1 Moving target indicator

We consider a moving target indicator (MTI) system with two pulses. This processing is based on the difference between echoes received from consecutive pulses. Let the received signal at the mth sensor for the first pulse transmitted at time t be denoted by $u_m(t)$. Similarly, the received signal from the second pulse transmitted at time $t + PRI$ be denoted by $u_m(t + PRI)$. The echoes generated from non-moving objects do not vary in their delay and phase from pulse to pulse. Hence, the resulting difference signal is zero and all echoes due to non-moving objects at time t are effectively suppressed.

Now, we consider that at instants t_0 and $t_0 + PRI$, the echoes of Z_1 moving objects are present. The resulting signal is a combination of the echoes of both signals and is given by

$$\begin{aligned}
\Delta u_m(t_0) &= u_m(t_0 + PRI) - u_m(t_0) \\
&= \sum_{z=1}^{Z_1} \beta_z(t_0 + PRI)\, e^{2\pi j \hat{f}_z(t_0+PRI)t_0 + j\phi_{m,z}(t_0+PRI)} - \\
&\quad \sum_{z=1}^{Z_1} \beta_z(t_0)\, e^{2\pi j \hat{f}_z(t_0)t_0 + j\phi_{m,z}(t_0)} + \\
&\quad n_m(t_0 + PRI) - n_m(t_0).
\end{aligned} \tag{2.10}$$

Note that echoes from non-moving objects are removed.

Assume $\hat{f}_z(t_0 + PRI) = \hat{f}_z(t_0)$, i.e the zth object is moving with the same velocity at time $t_0 + PRI$ and t_0. This is a valid approximation given the time scales under consideration and the range of Doppler frequencies resulting from occupant movements in indoor office environments. Let us first analyze the case of $\phi_{m,z}(t_0 + PRI) \approx \phi_{m,z}(t_0)$, i.e. the object is moving in the radial direction with respect to the sensor. The expression in (2.10) can then be further simplified into

$$\begin{aligned}
\Delta u_m(t_0) &= \sum_{z=1}^{Z_1} [\beta_z(t_0 + PRI) - \beta_z(t_0)] e^{2\pi j \hat{f}_z(t_0) t_0 + j\phi_{m,z}(t_0)} + \\
&\quad n_m(t_0 + PRI) - n_m(t_0) \\
&= \sum_{z=1}^{Z_1} [\beta_z(t_0 + PRI) - \beta_z(t_0)] e^{2\pi j \hat{f}_z(t_0) t_0 + j\phi_{m,z}(t_0)} + \\
&\quad n_m(t_0 + PRI) - n_m(t_0) \\
&= \sum_{z=1}^{Z_1} b_z \left[e^{j4\pi \frac{d_z(t_0+PRI)}{\lambda}} - e^{j4\pi \frac{d_z(t_0)}{\lambda}} \right] \times \\
&\quad e^{2\pi j \hat{f}_z(t_0) t_0 + j\phi_{m,z}(t_0)} + \\
&\quad n_m(t_0 + PRI) - n_m(t_0). \qquad (2.11)
\end{aligned}$$

As we can see from (2.11) the resulting signal has a gain given by

$$\begin{aligned}
e^{j4\pi \frac{d_z(t_0+PRI)}{\lambda}} - e^{j4\pi \frac{d_z(t_0)}{\lambda}} &= e^{j4\pi \frac{d_z(t_0)}{\lambda}} \left[e^{j4\pi \frac{d_z(t_0+PRI) - d_z(t_0)}{\lambda}} - 1 \right] \\
&= e^{j4\pi \frac{d_z(t_0)}{\lambda}} \left[e^{j4\pi \frac{v_z(t_0) PRI}{\lambda}} - 1 \right] \qquad (2.12)
\end{aligned}$$

where $v_z(t_0) = \frac{1}{PRI}(d_z(t_0 + PRI) - d_z(t_0))$ is the radial speed of the zth moving object during the interval $[t_0, t_0 + PRI]$.

From (2.12), we observe that some speeds are suppressed. Those are blind speeds which can not be detected. The first blind speed is given by

$$\begin{aligned}
4\pi \frac{v_{blind}\ PRI}{\lambda} &= 2\pi \\
v_{blind} &= \frac{\lambda}{2\ PRI}
\end{aligned}$$

Any integer multiple of v_{blind} will be suppressed.

In our system this speed is

$$\begin{aligned}
v_{blind} &= \frac{8.6}{2 \times 32} \\
&\approx 0.13 \text{ ms}^{-1}
\end{aligned}$$

The resulting power gain within one pulse duration for different speeds of a target is plotted in Fig. 2.8. It is observed that the power oscillates with respect to the

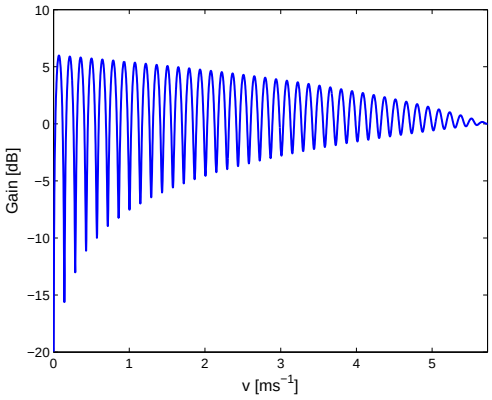

Figure 2.8: MTI power gain for different speeds

target's speed. Note that as the speed increases, the gain tends to zero. It is due to the fact that the two echoes are not overlapping anymore. For the general case of $\phi_{m,z}(t_0 + PRI) \neq \phi_{m,z}(t_0)$ a similar behavior as seen in Fig. 2.8 is expected. This situation causes an intermittent detection of a target. For assuring the detection of a target in those cases when it is attenuated by this method, a tracking of the target is performed after it is detected as explained further in Subsection 2.3.4.

2.3.2 Range processing

Let $\Delta u_m(t)$ be the output of the mth sensor after the MTI processor. Let f_s be the sampling rate for digitizing the signal and T_s the time over which we sample the signal ($T_s \leq PRI$).

We process the signal at every range $d(\rho)$ defined by (2.8). In other words, we analyze the signal during each time interval as shown in Fig. 2.9. The ρth time interval is given by

$$\left[\frac{(\rho-1)\,\Gamma}{f_s}\ ,\ \frac{\rho\Gamma}{f_s}\right]$$

where

$$\Gamma = \left\lfloor \frac{\Delta D f_s}{v_s} \right\rfloor$$

is the number of samples within the interval.

For each interval, we downmix the signal to baseband and apply a low-pass filter. The cutoff frequency of the filter determines which doppler frequencies are filtered out. The low-pass filter is implemented as the average of the signal over the analyzed interval. Hence, the cutoff frequency of the low-pass filter depends on the duration of the interval, Γ. The filter response for different speed of the occupant is shown in Fig. 2.10.

Note that the filter attenuates more than 3 dB the signal of a target moving with a speed higher than 2 ms^{-1}. Hence, we design the downmixing signal so as to compensate the attenuation for the speeds higher than 2 ms^{-1} and lower than v_{max}.

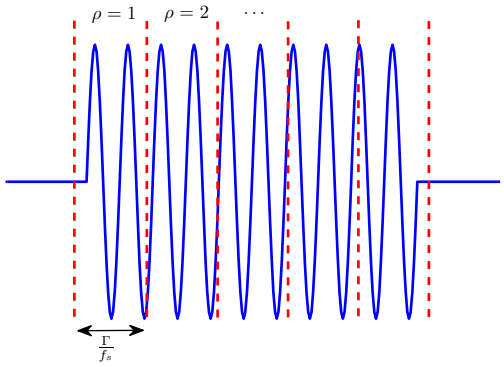

Figure 2.9: Processing interval per range bin

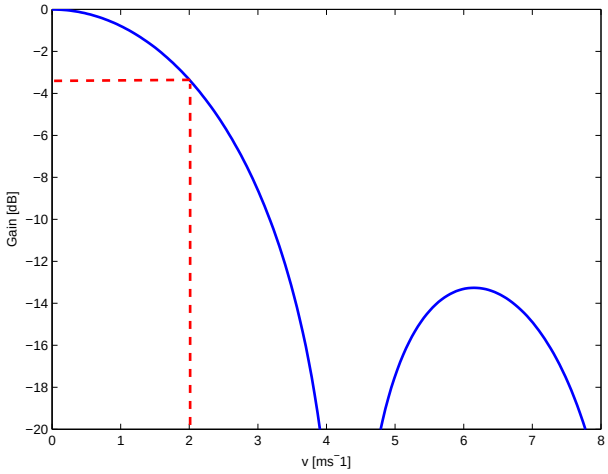

Figure 2.10: Gain of the filter for different speeds of the occupant

Let $g(t)$ be the downmixing signal denoted by

$$g(t) = e^{-2\pi j\left(f_c+\tilde{f}\right)t} - e^{-2\pi j\left(f_c-\tilde{f}\right)t}$$

where $\tilde{f}$ is a design parameter. The parameter $\tilde{f}$ is chosen so as to provide a similar maximum combined gain (MTI, downmixing and filtering) for any occupant moving with a speed lower than v_{max}.

We desire that all the peaks of the combined gain is above 0 dB for speeds lower than v_{max}. Hence, we chose $\tilde{f} = 690$ Hz for our application. The combined gain for different speeds of the occupant is shown in Fig. 2.11.

The gain after downmixing and filtering the signal for different speeds of the occupant is depicted in Fig. 2.12. It can be noted that for speeds below 1 ms^{-1}, the gain is lower than -3 dB. However, this is not a problem because the MTI processor provides a gain higher than 5 dB for these speeds.

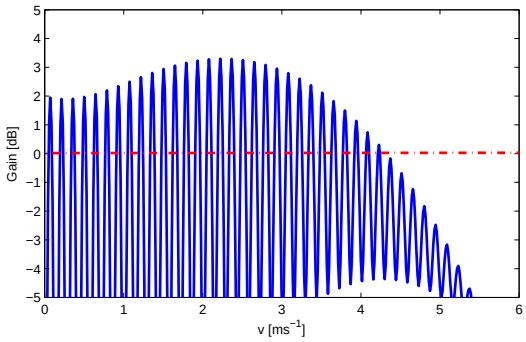

Figure 2.11: Combined gain (MTI, downmixing and filtering) for different speeds of the occupant

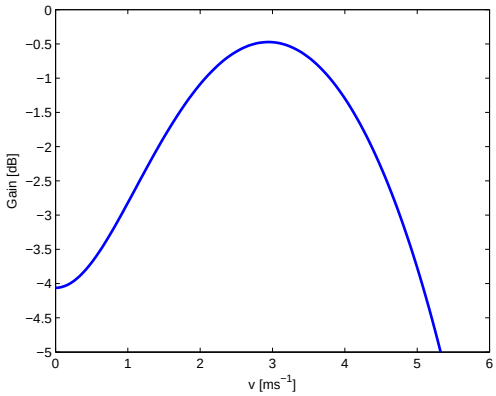

Figure 2.12: Gain of the signal after downmixing and filtering

Finally, the vector corresponding to the ρth processed range bin, $\hat{\boldsymbol{u}}(\rho)$, is given by

$$\hat{\boldsymbol{u}}(\rho) = \begin{bmatrix} \hat{u}_1(\rho) \\ \vdots \\ \hat{u}_M(\rho) \end{bmatrix} = \frac{1}{\Gamma} \sum_{\gamma=1}^{\Gamma} \begin{bmatrix} \Delta u_1 \left(\frac{\gamma-1+(\rho-1)\Gamma}{f_s} \right) g\left(\frac{\gamma-1}{f_s} \right) \\ \vdots \\ \Delta u_M \left(\frac{\gamma-1+(\rho-1)\Gamma}{f_s} \right) g\left(\frac{\gamma-1}{f_s} \right) \end{bmatrix}$$

Accordingly, the received power per range is given by

$$\Lambda(\rho) = \left[\frac{1}{M} \sum_{m=1}^{M} |\hat{u}_m(\rho)| \right]^2 . \tag{2.13}$$

The peaks of (2.13) correspond to possible targets. For each peak, we calculate the ratio of the received signal $\Lambda(\rho)$ to the noise level $\sigma^2(\rho)$ (Signal to Noise ratio, SNR). If the SNR is at least C_d dB, then a target is declared in that range bin. Next, we proceed to determine the DoAs for each range where a target was declared.

2.3.3 DoA processing

We perform the DoA processing in each range bin, ρ, where a target was declared in the previous subsection. A high-resolution beamforming algorithm (MVDR) is used to obtain the DoAs of the targets. The MVDR beamformer is given by

$$\boldsymbol{w}(\theta) = \frac{\boldsymbol{R}^{-1}\boldsymbol{a}(\theta)}{\boldsymbol{a}^H(\theta)\,\boldsymbol{R}^{-1}\boldsymbol{a}(\theta)} \tag{2.14}$$

where $\boldsymbol{R}$ is the covariance matrix of the received signal and $\boldsymbol{a}(\theta)$ is given by (2.2).

Assuming L ($L \leq M$) signals arrive with known angles θ_1, θ_2, ..., θ_L, respectively. If these signals are independent then the results obtained by the MVDR beamformer are highly accurate.

However, in the presence of multiple coherent signals, the performance of the MVDR is highly degraded. The degradation is owing to the cancelation of the desired signals. A way of overcoming this situation is by using

$$\boldsymbol{R} \equiv [\boldsymbol{a}(\theta_1), \ldots, \boldsymbol{a}(\theta_L)]\,[\boldsymbol{a}(\theta_1), \ldots, \boldsymbol{a}(\theta_L)]^H$$

in (2.14) in order to form the MVDR beamformer.

Since we do not know in advance the DoAs of the signals, we consider the following iterative procedure.

Let $\boldsymbol{DoA}^{(0)}$ denote the initial list containing DoAs given by

$$\boldsymbol{DoA}^{(0)} = \left[\hat{\theta}_1^{(0)}\right]$$

where $\hat{\theta}_1^{(0)}$ correspond to the highest peak of

$$\Lambda^{(0)}(\theta) = \left|\frac{1}{M}\boldsymbol{a}^H(\theta)\,\hat{\boldsymbol{u}}(\rho)\right|^2.$$

The list $\boldsymbol{DoA}^{(k)}$ at the kth iteration is given by

$$\boldsymbol{DoA}^{(k)} = \left[\hat{\theta}_1^{(k)}; \hat{\theta}_2^{(k)}; \ldots; \hat{\theta}_{L+1}^{(k)}\right].$$

Given the previous list $\boldsymbol{DoA}^{(k-1)}$ with L different DoAs, the new list is formed with the $L+1$ highest peaks of

$$\Lambda^{(k)}(\theta) = \left|\boldsymbol{w}^{(k)\,H}(\theta)\,\hat{\boldsymbol{u}}(\rho)\right|^2$$

where $\boldsymbol{w}^{(k)}(\theta)$ is given by (2.14) using the matrix

$$\begin{aligned}\boldsymbol{R}^{(k-1)} \;=\; & \left[\boldsymbol{a}\left(\hat{\theta}_1^{(k-1)}\right), \ldots, \boldsymbol{a}\left(\hat{\theta}_L^{(k-1)}\right)\right] \times \\ & \left[\boldsymbol{a}\left(\hat{\theta}_1^{(k-1)}\right), \ldots, \boldsymbol{a}\left(\hat{\theta}_L^{(k-1)}\right)\right]^H + \epsilon\boldsymbol{I}_M\end{aligned}$$

and $\boldsymbol{I}_M$ is an identity matrix of size $M \times M$. Diagonal loading with factor ϵ is used for achieving robustness against inaccuracies in the array response model [14], [15].

The procedure is repeated till $L = M$ or all the peaks have been found. These peaks correspond to the DoAs of the signals within the ρth distance bin. Note that the angles $\theta_1, \theta_2, \cdots, \theta_L$ can only take values from the discrete set defined in (2.9).

Finally, the received power at location (ρ, θ) is given by

$$\Lambda(\rho, \theta) = \left| \boldsymbol{w}^H(\theta)\, \hat{\boldsymbol{u}}(\rho) \right|^2 \tag{2.15}$$

where $\boldsymbol{w}$ is the beamformer obtained at the last iteration.

2.3.4 Target tracking

As we stated earlier in Subsection 2.3.1 there is an intermittent detection of a target in time. Particularly, when the target is still, the MTI processor suppress completely the target's signal. For coping with those situations a tracking and detection of targets is used [16]-[19].

We consider the model in [16], [17] and [18] for the dynamics of the trajectory of the occupant. The dynamics are modeled by a second order Markov chain with state $\boldsymbol{P}^{(t)}$ at time t given by

$$\boldsymbol{P}^{(t)} = \begin{bmatrix} \boldsymbol{p}^{(t)} \\ \boldsymbol{p}^{(t-1)} \end{bmatrix}.$$

where $\boldsymbol{p}^{(t)}$ is the occupant's location at time t.

Considering that the occupant's movement must satisfy constraints of temporal motion continuity, the predicted location $\bar{\boldsymbol{p}}^{(t)}$ is given by

$$\bar{\boldsymbol{p}}^{(t)} = \boldsymbol{p}^{(t-1)} + \left(\boldsymbol{p}^{(t-1)} - \boldsymbol{p}^{(t-2)}\right) \tag{2.16}$$

where $\boldsymbol{p}^{(t-1)}$ is the previous location and $\left(\boldsymbol{p}^{(t-1)} - \boldsymbol{p}^{(t-2)}\right)$ approximates the occupant's velocity.

The current new position follows a Gaussian distribution centered at the predicted position $\bar{\boldsymbol{p}}^{(t)}$. Thus,

$$\boldsymbol{P}^{(t)} = \boldsymbol{A}\boldsymbol{P}^{(t-1)} + \boldsymbol{b}\boldsymbol{u}^{(t)} \tag{2.17}$$

with

$$\boldsymbol{A} = \begin{bmatrix} 2 & -1 \\ 1 & 0 \end{bmatrix}, \qquad \boldsymbol{b} = \begin{bmatrix} 1 \\ 0 \end{bmatrix}$$

where $\boldsymbol{A}$ is the state propagation matrix and $\boldsymbol{u}^{(t)}$ is a zero mean white Gaussian noise vector with covariance $\boldsymbol{Q}_u = E\left[\boldsymbol{u}\boldsymbol{u}^H\right]$.

Additionally, we assume the following observation model

$$\tilde{\boldsymbol{p}}^{(t)} \;=\; \boldsymbol{p}^{(t)} + \boldsymbol{v}^{(t)} \tag{2.18}$$

where $\tilde{\boldsymbol{p}}^{(t)}$ is the observed location at time t and $\boldsymbol{v}^{(t)}$ is a zero mean white Gaussian noise vector with covariance $\boldsymbol{Q}_v = E\left[\boldsymbol{v}\boldsymbol{v}^H\right]$.

Given the trajectory model and observation model defined in (2.17) and (2.18) respectively, the probability that a target is observed at location $\tilde{\boldsymbol{p}}^{(t)}$ given its previous state $\boldsymbol{P}^{(t-1)}$ follows a normal distribution given by

$$p\left\{\tilde{\boldsymbol{p}}^{(t)}|\boldsymbol{P}^{(t-1)}\right\} \rightarrow \mathcal{N}\left(\bar{\boldsymbol{p}}^{(t)}, \boldsymbol{Q}\right) \tag{2.19}$$

where $\bar{\boldsymbol{p}}^{(t)}$ is defined by (2.16) and $\boldsymbol{Q} = \boldsymbol{Q}_u + \boldsymbol{Q}_v$.

After range and DoA processing, we obtain several measurements corresponding to the locations of the occupants, multipath and clutter. These Υ locations are compiled in the list $\boldsymbol{\mathcal{Z}}^{(t)}$ given by

$$\boldsymbol{\mathcal{Z}}^{(t)} = [\mathcal{Z}_1^{(t)}; \mathcal{Z}_2^{(t)}; \ldots; \mathcal{Z}_\Upsilon^{(t)}] = [\tilde{\boldsymbol{p}}_1^{(t)}; \tilde{\boldsymbol{p}}_2^{(t)}; \ldots; \tilde{\boldsymbol{p}}_\Upsilon^{(t)}]$$

where

$$\begin{aligned}
\tilde{\boldsymbol{p}}_\upsilon^{(t)} &= [\tilde{x}_\upsilon^{(t)}, \tilde{y}_\upsilon^{(t)}], \\
\tilde{x}_\upsilon &= \frac{v_s}{2}\tilde{\rho}_\upsilon \cos\left(\tilde{\theta}_\upsilon\right) - \frac{l}{2}, \\
\tilde{y}_\upsilon &= \frac{v_s}{2}\tilde{\rho}_\upsilon \sin\left(\tilde{\theta}_\upsilon\right)
\end{aligned}$$

correspond to the υth measured location.

We must consider two aspects with respect to these measurements. One aspect is that these locations may correspond to previous targets (e.g. occupant moving inside the room) or new targets (e.g. occupant entering the room). The second is that in practice, the sensor array receives multiple reflections from different parts of the human body corresponding to the occupant. These need to be combined to correspond to a single location.

For target tracking, we introduce a score vector as done in [19]. A score vector represents the past history of the targets. The algorithm for target tracking is as follows.

First, we relate each measurement in the list $\boldsymbol{\mathcal{Z}}^{(t)}$ to a previous target (if it is possible), i.e. we update the score vector $\overline{\boldsymbol{TBD}}^{(t)}$ of the measurements denoted by

$$\overline{\boldsymbol{TBD}}^{(t)} = [\overline{TBD}_1^{(t)}, \overline{TBD}_2^{(t)}, \ldots, \overline{TBD}_\Upsilon^{(t)}].$$

Assume Ξ targets have been detected at time $t-1$. The information of these targets is compiled in the list $\hat{\boldsymbol{\mathcal{P}}}^{(t-1)}$ with the states of the targets and the respective score vector $\boldsymbol{TBD}^{(t-1)}$,

$$\begin{aligned}
\hat{\boldsymbol{\mathcal{P}}}^{(t-1)} &= \left[\hat{\boldsymbol{P}}_1^{(t-1)};\ \hat{\boldsymbol{P}}_2^{(t-1)};\ \ldots;\ \hat{\boldsymbol{P}}_\Xi^{(t-1)}\right] \\
\boldsymbol{TBD}^{(t-1)} &= [TBD_1^{(t-1)}, TBD_2^{(t-1)}, \ldots, TBD_\Xi^{(t-1)}].
\end{aligned}$$

Then, the score of the υth measurement, $\overline{TBD}_\upsilon^{(t)}$, is updated by the equation

$$\overline{TBD}_\upsilon^{(t)} = F\{\tilde{\boldsymbol{p}}_\upsilon^{(t)}\} + \alpha_1 \max_\xi \left[p\left\{\tilde{\boldsymbol{p}}_\upsilon^{(t)}|\hat{\boldsymbol{P}}_\xi^{(t-1)}\right\} TBD_\xi^{(t-1)}\right]$$

where α_1 is a factor for controlling the past history taking values from $[0, 1]$. $p\{\}$ is the conditional probability as defined in (2.19). $F\{\}$ is the log-likelihood function of the received power denoted by

$$F\{x, y\} = 10 \log_{10} \left(\frac{\Lambda(\rho, \theta)}{\sigma^2(\rho, \theta)} \right)$$

where

$$\begin{aligned} \rho &= \frac{2}{v_s} \sqrt{\left(x + \frac{l}{2}\right)^2 + y^2}, \\ \theta &= \tan^{-1}\left(\frac{y}{x + \frac{l}{2}}\right), \end{aligned}$$

$\Lambda(\rho, \theta)$ is the received power given by (2.15) and $\sigma^2(\rho, \theta)$ is the noise level at the location (ρ, θ).

Note that if a measurement does not correspond to any previous target, the conditional probability $p\{\}$ tends to zero and so the score of that measurement is not updated with past history. In this case, the score is equal to

$$\overline{TBD}_v^{(t)} = F\{\tilde{\boldsymbol{p}}_v^{(t)}\}.$$

After updating the score vector, we need to combine the measurements which correspond to the same target to a single location.

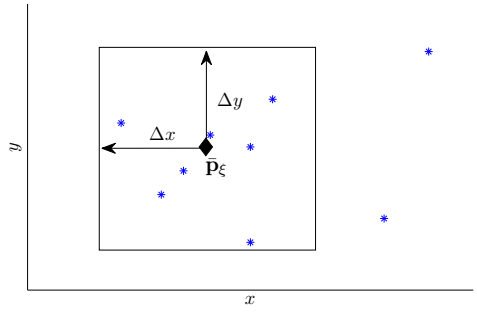

Figure 2.13: Plot of the measurements in xy-coordinate system

Let Δx and Δy be the dimensions of the area a person occupies in the xy-plane, respectively, as shown in Fig. 2.13. After combining the measurements, we obtain the compiled list $\boldsymbol{\mathcal{P}}^{(t)}$ with current state of the targets and the score vector $\boldsymbol{TBD}^{(t)}$ which are denoted respectively by

$$\begin{aligned} \hat{\boldsymbol{\mathcal{P}}}^{(t)} &= \left[\hat{\boldsymbol{P}}_1^{(t)}; \ldots; \hat{\boldsymbol{P}}_{\Xi+N}^{(t)}\right] \\ \boldsymbol{TBD}^{(t)} &= [TBD_1^{(t)}, \ldots, TBD_{\Xi+N}^{(t)}]. \end{aligned}$$

The first Ξ elements of the list $\hat{\boldsymbol{\mathcal{P}}}^{(t)}$ correspond to updated states from previous targets while the last N elements are states from new targets. Let $\hat{\boldsymbol{P}}_{\xi}^{(t-1)}$ be the state of a target at time $t-1$. The predicted location at time t of this target is denoted by

$$\bar{\boldsymbol{p}}_{\xi}^{(t)} = [\bar{x}_{\xi}^{(t)}, \bar{y}_{\xi}^{(t)}]$$

and calculated by

$$\bar{\boldsymbol{p}}_{\xi}^{(t)} = \hat{\boldsymbol{p}}_{\xi}^{(t-1)} + \left(\hat{\boldsymbol{p}}_{\xi}^{(t-1)} - \hat{\boldsymbol{p}}_{\xi}^{(t-2)}\right).$$

All the measured locations from the list $\boldsymbol{\mathcal{Z}}^{(t)}$ which are in the area surrounding the predicted location $\bar{\boldsymbol{p}}_{\xi}^{(t)}$ as shown in Fig. 2.13, i.e. in the set

$$\mathcal{A}_{\xi}^{(t)} \;=\; \left\{\tilde{\boldsymbol{p}}_{\upsilon}^{(t)} : |\tilde{x}_{\upsilon}^{(t)} - \bar{x}_{\xi}^{(t)}| \leq \Delta x \;\text{ and }\; |\tilde{y}_{\upsilon}^{(t)} - \bar{y}_{\xi}^{(t)}| \leq \Delta y;\; \upsilon = 1, \ldots, \Upsilon\right\},$$

are weighted and combined into one single estimated location $\hat{\boldsymbol{p}}_{\xi}^{(t)}$ by

$$\hat{\boldsymbol{p}}_{\xi}^{(t)} \;=\; \frac{1}{\mathcal{K}_{\xi}^{(t)}} \sum_{\upsilon \,:\, \tilde{\boldsymbol{p}}_{\upsilon}^{(t)} \in \mathcal{A}_{\xi}^{(t)}} \overline{TBD}_{\upsilon}^{(t)} \tilde{\boldsymbol{p}}_{\upsilon}^{(t)}$$

where

$$\mathcal{K}_{\xi}^{(t)} = \sum_{\upsilon \,:\, \tilde{\boldsymbol{p}}_{\upsilon}^{(t)} \in \mathcal{A}_{\xi}^{(t)}} \overline{TBD}_{\upsilon}^{(t)}$$

is a normalizing factor.

The current state $\hat{\boldsymbol{P}}_{\xi}^{(t)}$ is given by

$$\hat{\boldsymbol{P}}_{\xi}^{(t)} = \begin{bmatrix} \hat{\boldsymbol{p}}_{\xi}^{(t)} \\ \hat{\boldsymbol{p}}_{\xi}^{(t-1)} \end{bmatrix}$$

with score

$$TBD_{\xi}^{(t)} = \max_{\upsilon \,:\, \tilde{\boldsymbol{p}}_{\upsilon}^{(t)} \in \mathcal{A}_{\xi}^{(t)}} \overline{TBD}_{\upsilon}^{(t)}.$$

Some comments regarding this step. If for a given ξ, the list $\mathcal{A}_{\xi}^{(t)}$ is an empty set, we proceed to include the corresponding location $\hat{\boldsymbol{p}}_{\xi}^{(t)}$ in the current estimated state list as

$$\begin{aligned} \hat{\boldsymbol{P}}_{\xi}^{(t)} \;&=\; \begin{bmatrix} \hat{\boldsymbol{p}}_{\xi}^{(t-1)} \\ \hat{\boldsymbol{p}}_{\xi}^{(t-1)} \end{bmatrix} \\ TBD_{\xi}^{(t)} \;&=\; \alpha_2 TBD_{\xi}^{(t-1)} \end{aligned}$$

where α_2 is a factor for controlling the past history in the score vector with values in the range $[0, 1)$.

Let

$$\tilde{\boldsymbol{\mathcal{Z}}}^{(t)} = [\tilde{\mathcal{Z}}_1^{(t)}; \tilde{\mathcal{Z}}_2^{(t)}; \ldots; \tilde{\mathcal{Z}}_N^{(t)}]$$

be a list with N new measured locations (i.e. measurements that do not correspond to previous targets) denoted by

$$\tilde{\boldsymbol{\mathcal{Z}}}^{(t)} = \left\{ \tilde{\boldsymbol{p}}_\upsilon^{(t)} : \tilde{\boldsymbol{p}}_\upsilon^{(t)} \notin \mathcal{A}_\xi^{(t)}; \quad \xi = 1, \ldots, \Xi; \ \upsilon = 1, \ldots, \Upsilon \right\}.$$

The nth element of this list, $\tilde{\mathcal{Z}}_n^{(t)}$, is added to the list $\hat{\boldsymbol{\mathcal{P}}}^{(t)}$ as

$$\begin{aligned} \hat{\boldsymbol{P}}_{\Xi+n}^{(t)} &= \begin{bmatrix} \tilde{\mathcal{Z}}_n^{(t)} \\ \tilde{\mathcal{Z}}_n^{(t)} \end{bmatrix} \\ TBD_{\Xi+n}^{(t)} &= \overline{TBD}_n^{(t)} \end{aligned}$$

where $\overline{TBD}_n^{(t)}$ is the score corresponding to the location $\tilde{\mathcal{Z}}_n^{(t)}$.

If the score $TBD_i^{(t)}$ of the ith current estimated state is higher than a defined detection threshold C_{th}, then an occupant is detected in that location.

Let $\tilde{\boldsymbol{p}}_i^{(t)}$ be the location where an occupant has been previously detected. This location is discarded if the corresponding score $TBD_i^{(t)}$ is below the threshold C_{th} for a period of time longer than T_{th}.

2.3.5 Multipath mitigation

The effect of multipath has not been considered so far. The key observation we use is that in a number of instances, multipath results in estimated locations that are infeasible. For example, they may result in locations that fall outside the dimensions of the room as depicted in Fig. 2.5. Hence, we can discard these location using the following criterion

$$|x| > \frac{l}{2} \text{ or } |y| > \frac{w}{2}. \tag{2.20}$$

2.4 Conclusions

In this chapter, we proposed an ultrasonic sensor array solution for indoor localization. We provided 2-D localization by using the time of flight and DoA of the received signals. We coped with DoA estimation for multiple coherent signals by implementing an MVDR based iterative procedure. Multipath was mitigated by identifying and discarding infeasible locations.

3 Illumination Control

In this chapter, we present an illumination control algorithm for an LED lighting system. First, we describe the LED lighting system and also present LED illumination models. Next, the design of energy-efficient illumination control is formulated as an inequality constrained optimization problem. We analyze this optimization problem as a linear program. A simplex algorithm is employed to obtain the LED dimming levels. Under this illumination control algorithm, the performance of the LED system is evaluated using LUXEON LED models.

Illumination achieved by an LED system depends on the illumination radiation pattern and the dimming level of the individual LEDs. A Lambertian function [20], [21] is commonly used to model the broad beam illumination pattern of an LED. The dimming level thus provides the degree of freedom to control illumination patterns realized by an LED system.

The problem of illumination rendering has been treated in [4], [22]. In [23], the idea of modulating LED illumination pulses using code division multiplexing was presented as a way to facilitate determining individual illumination contributions at a receiver. Solutions based on frequency division multiplexing as a means to determine (and control) individual LED dimming levels have been treated in [24] and [25].

We shall assume that the locations of the occupants have been determined by the ultrasonic sensor array. It is desired to achieve uniform illumination at a prescribed level surrounding these locations. In unoccupied areas, it is desired to have a minimal illumination level. Both levels are chosen so as to meet required illumination norms. The total power consumption of the LED lighting system is desired to be minimal. In practice, uniform illumination means that variations in the illumination level must be below a certain threshold. The distortion in illumination pattern at location (x, y) with respect to a target illuminance level L is characterized by the illuminance contrast, as given by Weber's law [26, pp. 71],

$$C\left(E\left(x,y;h\right),L\right) \;=\; \frac{E\left(x,y;h\right)-L}{L} \tag{3.1}$$

where $E\left(x,y;h\right)$ is the illuminance at point (x,y) and distance h.

3.1 LED lighting system

LEDs on a uniformly spaced grid in the ceiling of the room supply the illumination. Let N_x and N_y be the number of LEDs distributed along the length and width respectively

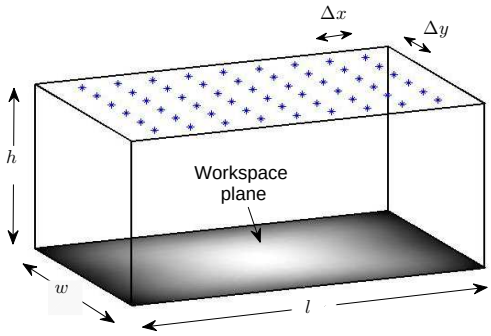

Figure 3.1: Illumination of an LED lighting system

of the room ceiling with separation

$$\begin{aligned} \Delta x &= \frac{l}{N_x}, \\ \Delta y &= \frac{w}{N_y}. \end{aligned}$$

For convenience, a coordinate system is assumed with the origin at the center of the ceiling.

The location of the ith LED is given by the coordinate pair (x_i, y_i) where

$$\begin{aligned} x_i &= \left(\alpha - \frac{N_x - 1}{2}\right)\Delta x, \quad \alpha = (i-1) \bmod N_x \\ y_i &= \left(\beta - \frac{N_y - 1}{2}\right)\Delta y, \quad \beta = \left\lfloor \frac{i-1}{N_x} \right\rfloor \\ &\text{for} \quad i = 1, 2, \cdots, N_x N_y. \end{aligned}$$

All the measurements of illuminance are taken at a plane parallel to the ceiling located at a distance h, measured perpendicular from the LEDs' plane. This distance represents a normal height for a working place, e.g. a desk.

As such, there are two planes (as depicted in Fig. 3.1) - one in which the LEDs are placed and the other is the workspace plane. We will not introduce a z-coordinate to distinguish the two planes for clarity of exposition since the difference will be clear from the context.

3.2 Problem formulation

We now mathematically formalize the illumination control problem.

Denote by $\boldsymbol{d}$, the $N_x N_y \times 1$ dimming vector, given by

$$\boldsymbol{d} = \left[d_1, \ldots, d_{N_x N_y}\right],$$

where $0 \leq d_i \leq 1$ is the dimming level of the ith LED. $d_i = 0$ means that the LED is dimmed off while $d_i = 1$ represents that the LED is at its maximum illumination.

Given J known locations (x_j, y_j) of occupants, it is desired to have a uniform illumination level, L_{max}, in regions around the occupant locations. Denote this whole region by R_o:

$$R_o = \{(x, y) : || (x, y) - (x_j, y_j) ||_2 \leq r_0, j = 1, \ldots, J\} \tag{3.2}$$

and its area by Ω. The constant r_0 may be chosen as per workspace norms and occupant comfort. Thus at any point in R_o, we have the contrast between the total illumination and L_{max} to be lower than a prescribed contrast C_{th}. Furthermore, the mean illumination level over R_0 is desired to be L_{max}. Outside region R_o, it is desired that the illumination level be at least L_{min}.

We seek to minimize the total power consumed by the lighting system under the illumination constraints in the occupied and unoccupied regions. Formally, we want to determine the optimum dimming vector $\boldsymbol{d}^\star$ to solve

$$\begin{aligned} \boldsymbol{d}^\star &= \arg\min_{\boldsymbol{d}} \sum_{i=1}^{N_x N_y} P_i (d_i) \\ \text{s.t.} \quad & \begin{cases} |C (E_T (x, y, \boldsymbol{d}; h), L_{max}) | \leq C_{th}, \\ \qquad\qquad \forall (x, y) \in R_o \\ E_T (x, y, \boldsymbol{d}; h) \geq L_{min}, \\ \qquad\qquad \forall (x, y) \notin R_o \\ \frac{1}{\Omega} \int_{(x,y)\in R_o} E_T (x, y, \boldsymbol{d}; h) \, \partial x \partial y = L_{max} \\ 0 \leq d_i \leq 1, \qquad i = 1, \ldots, N_x N_y. \end{cases} \end{aligned} \tag{3.3}$$

Here, P_i is the average power consumption of the ith LED at dimming level d_i. $E_T (x, y, \boldsymbol{d}; h)$ is the total illuminance at point (x, y) and distance h resulting by using dimming vector $\boldsymbol{d}$.

Some comments are in order regarding the optimization problem in (3.3). Note that in the region outside R_o, we only require an illumination level of at least L_{min}, which is different from the requirement of uniform illumination of L_{max} inside R_o. This is due to the practical reason that it is not possible to achieve uniform illumination in this region owing to edge effects (e.g., on the boundaries outside R_o and near the walls). Further, we shall assume a feasible solution exists for problem (3.3). That is, the LED system is designed in the first place such that illumination control can be done as per (3.3).

3.2.1 Power consumption

The illumination intensity of an LED is typically controlled using pulse width modulation (PWM) [27]. The dimming level d_i is in fact the duty cycle of the PWM waveform. Hence, the average power consumed by the ith LED over one waveform cycle is

$$P_i(d_i) = d_i P_{on} + (1 - d_i) P_{off} \tag{3.4}$$

where P_{on} and P_{off} are the power consumptions while the LED is on and off, respectively. In practice, $P_{off} = 0$. Hence

$$P_i(d_i) = d_i P_{on}.$$

Then, the total power, P_T, consumed by the lighting system is the summation of the average power of each LED:

$$P_T = \sum_{i=1}^{N_x N_y} d_i P_{on}. \tag{3.5}$$

Thus, minimizing the total power consumption is equivalent to minimizing the sum of the dimming levels of the LEDs,

$$\arg\min_{\boldsymbol{d}} \sum_{i=1}^{N_x N_y} P_i\left(d_i\right) \equiv \arg\min_{\boldsymbol{d}} \sum_{i=1}^{N_x N_y} d_i. \tag{3.6}$$

3.2.2 Illumination pattern model

A widely used model for the illumination pattern of an LED is the generalized Lambertian function [20], [21]. The illuminance, in the workspace plane, at location (x, y) and a distance h for a single LED located at (x_i, y_i) is

$$E_i(x, y; h) = A\left[1 + \frac{||\,(x, y) - (x_i, y_i)\,||_2^2}{h^2}\right]^{-\frac{m+3}{2}} \tag{3.7}$$

with

$$A = \frac{(m+1)\,A_0}{2\pi h^2}$$

where A_0 is the luminous flux of the light and m is the Lambertian mode ($m > 0$). This mode is related to the semiangle of the light beam at half power, $\Phi_{\frac{1}{2}}$, determined by

$$m = -\frac{\ln(2)}{\ln\left(\cos\left(\Phi_{\frac{1}{2}}\right)\right)}.$$

The overall illumination at position (x, y) is then equal to the combined contribution of every LED. Thus, with the ith LED at dimming level d_i and the illumination pattern in (3.7), the total illuminance is written as

$$\begin{aligned} E_T\left(x, y, \boldsymbol{d}; h\right) &= \sum_{i=1}^{N_x N_y} d_i E_i(x, y; h) \\ &= A \sum_{i=1}^{N_x N_y} d_i \left[1 + \frac{||\,(x, y) - (x_i, y_i)\,||_2^2}{h^2}\right]^{-\frac{m+3}{2}}. \end{aligned} \tag{3.8}$$

Note that the above model implicitly assumes a "black room" and neglects reflections of light occurring in the room. In practice, these contributions need to be accounted for in the overall illumination. This can be done by incorporating a reflection model for a given room [28] or by actually measuring light intensities using appropriate sensors.

Now, using (3.6) and (3.8), our original problem (3.3) can be rewritten as

$$\begin{aligned} \boldsymbol{d}^\star &= \arg\min_{\boldsymbol{d}} \sum_{i=1}^{N_x N_y} d_i \\ \text{s.t.} \quad & \begin{cases} |\sum_{i=1}^{N_x N_y} d_i E_i(x,y;h) - L_{max}| \leq L_{max} C_{th} \\ \qquad \forall\, (x,y) \in R_o \\ \sum_{i=1}^{N_x N_y} d_i E_i(x,y;h) \geq L_{min}, \\ \qquad \forall\, (x,y) \notin R_o \\ \sum_{i=1}^{N_x N_y} d_i \left[\frac{1}{\Omega} \int_{(x,y)\in R_o} E_i(x,y;h) \partial x \partial y \right] = L_{max} \\ 0 \leq d_i \leq 1, \qquad i = 1, \ldots, N_x N_y. \end{cases} \end{aligned} \tag{3.9}$$

3.2.3 Illumination uniformity

The feasibility of obtaining a uniform illumination pattern depends on the beamwidth of the LEDs and the amount of overlap of their patterns, i.e. the separation amongst LEDs.

There is a trade-off between these two parameters. When the LEDs are on a uniform grid, with an illumination pattern as defined by (3.7), the maximum separation between two consecutive LEDs ($\Delta = \Delta x = \Delta y$) that ensures a uniform illumination is given by the approximation [29]

$$\Delta = h \sqrt{\frac{1.2125}{m - 3.349}} \tag{3.10}$$

for $N_x > 4$ and $N_y > 4$ and $m > 30$. This gives us an upper threshold for the maximum separation amongst LEDs to ensure that a uniform illumination is feasible.

3.3 Algorithm for illumination control

Note that the objective function as well as the constraints of the optimization problem in (3.9) are linear in $\{d_i\}$.

To write (3.9) in the standard form of a linear optimization problem [30, pp. 146], we first discretize the constraints. To do this, we divide the workspace plane into a uniform spaced grid with N_l and N_w number of points along the length and width of the room, respectively. The separation between points is given by

$$\begin{aligned} \Delta w &= \frac{w}{N_w}, \\ \Delta l &= \frac{l}{N_l}. \end{aligned}$$

The kth location is given by the coordinate pair (x_k, y_k) where

$$\begin{aligned} x_k &= \left(\gamma - \frac{N_l - 1}{2}\right)\Delta l, \quad \gamma = (k-1) \bmod N_l \\ y_k &= \left(\zeta - \frac{N_w - 1}{2}\right)\Delta w, \quad \zeta = \left\lfloor \frac{k-1}{N_l} \right\rfloor \\ &\text{for} \quad k = 1, 2, \cdots, N_w N_l. \end{aligned}$$

Let R_f be the region within which the target illumination levels are feasible. Outside this region (in practice, this corresponds to points near the walls of the office) those levels are not achievable owing to edge effects and thus the constraints at these points are not considered.

Furthermore, let us define two discrete sets of coordinate pairs $\mathcal{U}$ and $\mathcal{V}$ given by

$$\begin{aligned} \mathcal{U} &= \{(x_k, y_k) : (x_k, y_k) \in R_o \text{ and } (x_k, y_k) \in R_f\}, \\ &\quad k = 1, \ldots, N_w N_l; \\ \mathcal{V} &= \{(x_k, y_k) : (x_k, y_k) \notin R_o \text{ and } (x_k, y_k) \in R_f\}, \\ &\quad k = 1, \ldots, N_w N_l. \end{aligned}$$

Let U and V be the number of coordinate pairs in the sets $\mathcal{U}$ and $\mathcal{V}$, respectively. The uth or vth coordinate pair (x, y) in $\mathcal{U}$ or $\mathcal{V}$ is denoted by $\mathcal{U}_u$ or $\mathcal{V}_v$, respectively.

Rewriting the constraints in (3.9) and evaluating the constraints in their respective sets, we obtain

$$\begin{aligned} \sum_{i=1}^{N_x N_y} d_i E_i(\mathcal{U}_u; h) &\leq L_{max} C_{th} + L_{max}, \qquad u = 1, \ldots, U \\ -\sum_{i=1}^{N_x N_y} d_i E_i(\mathcal{U}_u; h) &\leq L_{max} C_{th} - L_{max}, \qquad u = 1, \ldots, U \\ -\sum_{i=1}^{N_x N_y} d_i E_i(\mathcal{V}_v; h) &\leq -L_{min}, \qquad v = 1, \ldots, V \\ \sum_{i=1}^{N_x N_y} d_i \left[\frac{1}{U}\sum_{u=1}^{U} E_i(\mathcal{U}_u; h)\right] &= L_{max}. \end{aligned} \tag{3.11}$$

Using (3.11), the optimization problem of (3.9) can be written in matrix form as

$$\begin{aligned} \boldsymbol{d}^\star &= \arg\min_{\boldsymbol{d}} \mathbf{1}^T_{N_x N_y \times 1} \boldsymbol{d} \\ \text{s.t.} \quad &\begin{cases} \boldsymbol{M}\boldsymbol{d} \leq \boldsymbol{b} \\ \boldsymbol{n}^T \boldsymbol{d} = L_{max} \\ 0 \leq d_i \leq 1, \quad i = 1, \ldots, N_x N_y \end{cases} \end{aligned} \tag{3.12}$$

where $\mathbf{1}_{N\times 1}$ is the vector $[1,1,\ldots,1]^T$ of size $N\times 1$ and

$$\boldsymbol{M} = \begin{bmatrix}\boldsymbol{M}_1\\ \boldsymbol{M}_2\\ \boldsymbol{M}_3\end{bmatrix}, \qquad \boldsymbol{b} = \begin{bmatrix}\boldsymbol{b}_1\\ \boldsymbol{b}_2\\ \boldsymbol{b}_3\end{bmatrix}, \qquad \boldsymbol{n} = \frac{1}{U}\sum_{u=1}^{U}\boldsymbol{f}_u$$

with

$$\boldsymbol{M}_1 = \begin{bmatrix}\boldsymbol{f}_1^T\\ \vdots\\ \boldsymbol{f}_U^T\end{bmatrix}, \qquad \boldsymbol{M}_2 = -\boldsymbol{M}_1, \qquad \boldsymbol{M}_3 = \begin{bmatrix}-\boldsymbol{g}_1^T\\ \vdots\\ -\boldsymbol{g}_V^T\end{bmatrix}$$

and

$$\begin{aligned}
\boldsymbol{f}_u &= [E_1(\mathcal{U}_u;h), E_2(\mathcal{U}_u;h), \cdots, E_{N_xN_y}(\mathcal{U}_u;h)]^T,\\
&\qquad u=1,\ldots,U\ ;\\
\boldsymbol{g}_v &= [E_1(\mathcal{V}_v;h), E_2(\mathcal{V}_v;h), \cdots, E_{N_xN_y}(\mathcal{V}_v;h)]^T,\\
&\qquad v=1,\ldots,V\ ;\\
\boldsymbol{b}_1 &= (L_{max}C_{th}+L_{max})\,\mathbf{1}_{U\times 1};\\
\boldsymbol{b}_2 &= (L_{max}C_{th}-L_{max})\,\mathbf{1}_{U\times 1};\\
\boldsymbol{b}_3 &= -L_{min}\mathbf{1}_{V\times 1}.
\end{aligned}$$

We now use slack variables [30, pp. 147] to transform the inequality constraints $\boldsymbol{M}\boldsymbol{d}\leq\boldsymbol{b}$ into equality constraints. Let the $(2U+V)\times 1$ vector of slack variables $\boldsymbol{s}$ be written as

$$\begin{aligned}
\boldsymbol{s} &= [s_1, s_2, \ldots, s_{2U+V}]^T\\
&\qquad s_q\geq 0, \quad q=1,\ldots,2U+V.
\end{aligned}$$

Hence, (3.12) can be posed as

$$\begin{aligned}
\boldsymbol{d}^\star &= \arg\min_{\boldsymbol{d}} \mathbf{1}_{N_xN_y\times 1}^T\boldsymbol{d}\\
\text{s.t.}\quad &\begin{cases}
\boldsymbol{M}\boldsymbol{d}+\boldsymbol{s}=\boldsymbol{b}\\
\boldsymbol{n}^T\boldsymbol{d}=L_{max}\\
0\leq d_i\leq 1, \quad i=1,\ldots,N_xN_y\\
s_q\geq 0, \quad q=1,\ldots,2U+V.
\end{cases}
\end{aligned} \tag{3.13}$$

Now our problem is in the standard form of a linear optimization problem with an additional upper bound for the variables $\{d_i\}$. For such problems, there are known efficient methods such as the simplex algorithm for obtaining an exact solution [31].

The solution of (3.13) obtained from the simplex algorithm results in continuous values for d_i lying between 0 and 1. As a final step, we discretize the resulting vector $\boldsymbol{d}^\star$. Assuming D levels for dimming an LED, we proceed to map each element of $\boldsymbol{d}^\star$ to the nearest dimming level (multiple of $\frac{1}{D}$). It is clear that this final step introduces an error in the solution which is inversely proportional to the number of levels D (see also the following section). For a high resolution level D, this error is negligible.

3.3.1 Computational complexity

In practice, the simplex method converges in less than $3Q$ iterations [32, pp. 114], where Q is the number of constraints (here, $Q = N_x N_y + 2U + V + 1$). In comparison, a full search method with a resolution of D levels for dimming the LEDs requires $D^{N_x N_y}$ iterations. Hence, a full search algorithm is unfeasible to use even when the number of LEDs is moderately large.

3.4 Numerical example

Parameter	Value
l [m]	6
w [m]	4
h [m]	2
L_{max} [lx]	500
L_{min} [lx]	300
r_0 [m]	1

Table 3.1: Indoor lighting parameters

We consider a typical indoor office scenario, with parameters shown in Table 3.1. The illumination lighting parameters comply with the recommendations of the European Committee for Standardization [33].

Parameter	Value
$\Phi_{\frac{1}{2}}$ [degrees]	60
Lambertian mode (m)	1
Luminous Flux (A_0) [lm]	180
Maximum Illuminance (A) per LED [lx]	14.3
Power Consumed (P_{on}) per LED [W]	2.24

Table 3.2: LED parameters

The parameters from Luxeon Rebel [20], which produces a Lambertian radiation pattern with $\Phi_{\frac{1}{2}} = 60$ degrees, are chosen for testing. These values are listed in Table 3.2. A single LED provides approximately 14.3 lx in the axis direction. Hence, the radiation pattern of the ith LED over the workspace plane is given by

$$E_i^{(60)}(x, y; h = 2) \quad = \quad 14.3 \left[1 + \frac{|| (x, y) - (x_i, y_i) ||_2^2}{4}\right]^{-2}.$$

Additionally, two other beam widths are tested. We consider the use of lenses for narrowing the beam. Most commercial lenses offer different beamwidths, from around 5 to 40 degrees, with different gains in illuminance [34].

$\Phi_{\frac{1}{2}}$ [degrees]	Gain Factor	Lambertian Mode (m)	Maximum Illuminance (A) per LED [lx]
10.5	4	41	180
18	2	14	90

Table 3.3: Maximum illuminance per LED using lenses

Nevertheless, only medium and broad beams are considered. Narrow beams are excluded due to the fact that in those cases the best choice of dimming levels is the trivial solution of turning on the LEDs in the surrounding of the occupant to achieve uniform illumination and dimming off the others to maintain the minimum level L_{min}. A summary of the maximum illuminance per LED using lenses with medium and broad angles $\Phi_{\frac{1}{2}}$ is shown in Table 3.3 [34]. The illumination patterns with $\Phi_{\frac{1}{2}} = 10.5$ and 18 degrees are respectively given by

$$\begin{aligned} E_i^{(10.5)}(x, y; h = 2) &= 180\left[1 + \frac{||(x, y) - (x_i, y_i)||_2^2}{4}\right]^{-22} \\ E_i^{(18)}(x, y; h = 2) &= 90\left[1 + \frac{||(x, y) - (x_i, y_i)||_2^2}{4}\right]^{-\frac{17}{2}}. \end{aligned}$$

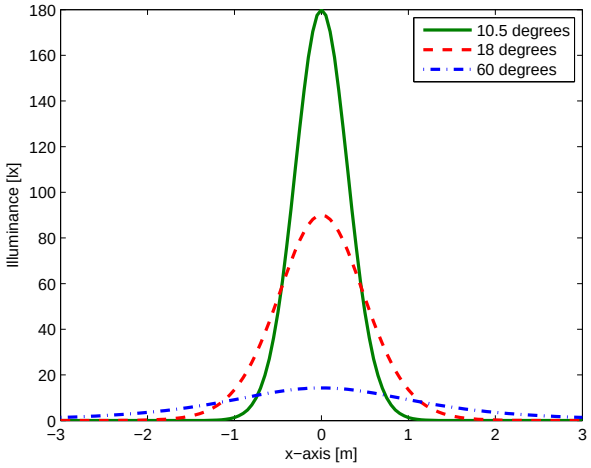

Figure 3.2: Illuminance pattern for different beamwidths

The corresponding patterns for $\Phi_{\frac{1}{2}}$ of 10.5, 18 and 60 degrees are shown in Fig. 3.2.

For dimming the LED, a resolution of 8 bits is chosen. This allows $D = 256$ different levels of illumination per LED. Furthermore, the error introduced in the calculated contrast is low. The error in the resulting contrast within R_0 for different bit resolutions is shown in Fig. 3.3. This error is calculated with an occupant located at the center of the room and $\Phi_{\frac{1}{2}} = 60$ degrees.

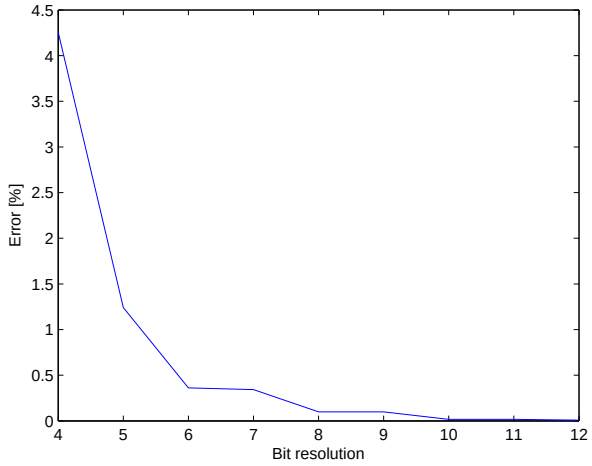

Figure 3.3: Error in contrast for different bit resolutions

$\Phi_{\frac{1}{2}}$ [degrees]	Maximum Separation ($\Delta = \Delta x = \Delta y$) [m]
10.5	0.359
18	0.583
60	1.287

Table 3.4: Maximum separation amongst LEDs

The separation of the LEDs is chosen in a way that allows to render a uniform illumination distribution across the plane. Thus, using (3.10), the maximum separation ($\Delta = \Delta x = \Delta y$) for each case is calculated. These results are shown in Table 3.4.

Parameter	Value
$\Delta x = \Delta l$ [m]	0.3
$\Delta y = \Delta w$ [m]	0.3
$N_x = N_l$	20
$N_y = N_w$	13

Table 3.5: Additional parameters of LED lighting system

The maximum separation is chosen as $\Delta = 0.3$ m. That means

$$\begin{aligned} N_x &= \frac{6}{0.3} \approx 20, \\ N_y &= \frac{4}{0.3} \approx 13 \end{aligned}$$

which in total represents 260 LEDs distributed over a uniform grid on the ceiling.

The constraints are evaluated at the same coordinate pairs (x, y) of the LEDs. These parameters are summarized in Table 3.5.

3.4.1 Performance comparison

We compare our proposed system and method (labeled, SM-2) with a system that renders uniform illumination at L_{max} across the whole room (labeled, SM-1[1]). The metric for comparison is the power consumed calculated from (3.5), while additionally considering the contrasts achieved.

We shall consider two values for the contrast threshold, C_{th}. One value is a tighter choice of $C_{th} = 0.05$ so as to provide a higher uniformity in illumination. The other is $C_{th} = 0.3$ which is as per the recommended limit of [33].

$\Phi_{\frac{1}{2}}$ [degrees]	10.5	18	60
Maximum contrast (SM-1)	0.05	0.05	0.05
Maximum contrast (SM-2)	0.05	0.05	0.05
Power (SM-1) [W]	277.63	233.32	331.86
Power (SM-2) [W]	184.80	156.85	205.52
Reduction in Power [%]	33.43	32.77	38.07

Table 3.6: Performance comparison of SM-1 and SM-2 (C_{th}=0.05)

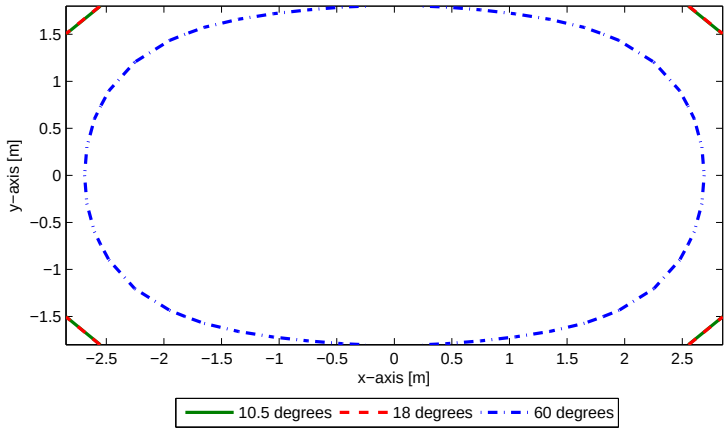

Figure 3.4: Region R_f for different angles $\Phi_{\frac{1}{2}}$ and $C_{th} = 0.05$

We first consider a single occupant located at the center of the office room, with $C_{th} = 0.05$. Results comparing SM-1 and SM-2 for this scenario are shown in Table 3.6. In Fig. 3.4, we depict the feasible region R_f for different values of $\Phi_{\frac{1}{2}}$ under SM-2. The obtained illumination patterns for each $\Phi_{\frac{1}{2}}$ are plotted in Figs. 3.5, 3.6 and 3.7,

[1]The dimming levels are optimized under SM-1 for minimum power consumption subject to a maximum contrast C_{th} and mean illumination level L_{max} over R_f.

respectively. As indicated in Table 3.6, in all three cases, the contrast is kept below the threshold of 0.05. With SM-2, we observe power savings higher than 32% in comparison to SM-1.

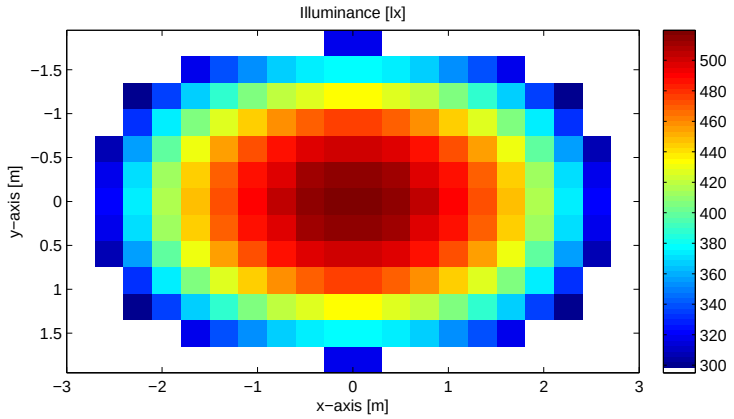

Figure 3.5: Illuminance pattern under SM-2 ($\Phi_{\frac{1}{2}} = 60$ degrees, C_{th}=0.05)

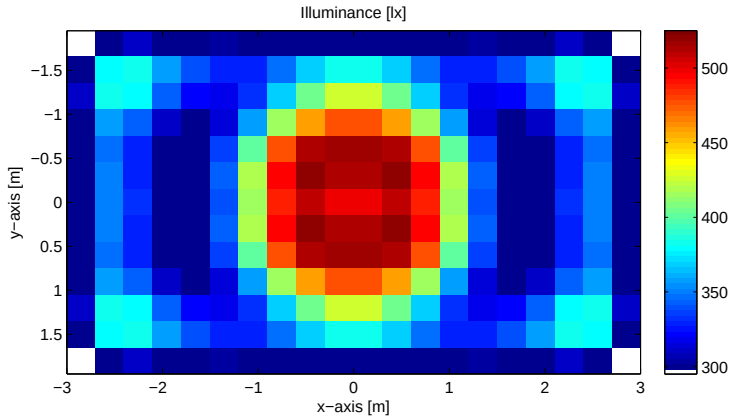

Figure 3.6: Illuminance pattern under SM-2 ($\Phi_{\frac{1}{2}} = 18$ degrees, C_{th}=0.05)

Additionally, with $\Phi_{\frac{1}{2}} = 60$ degrees, the dimming levels for an occupant located at the center of the office room for SM-2 and SM-1 are plotted in Figs. 3.8 and 3.9, respectively. We observe close to the borders a larger number of LEDs at a high dimming level with SM-1 than with SM-2.

Next, with $\Phi_{\frac{1}{2}} = 60$ degrees, we consider the performance of SM-2 with varying locations of the occupant. Due to symmetry, results are shown corresponding to locations where $x \geq 0$ and $y \geq 0$.

The illumination uniformity obtained within R_0 and power savings are shown in Fig. 3.10 and 3.11, respectively. As can be seen, the uniformity is maintained below 0.05 and the total power saving is more than 30%. The lowest power saving is obtained close to the corners of the room because fewer LEDs are contributing to the illumination at those locations. Thus, more LEDs need to be at higher illumination levels to illuminate

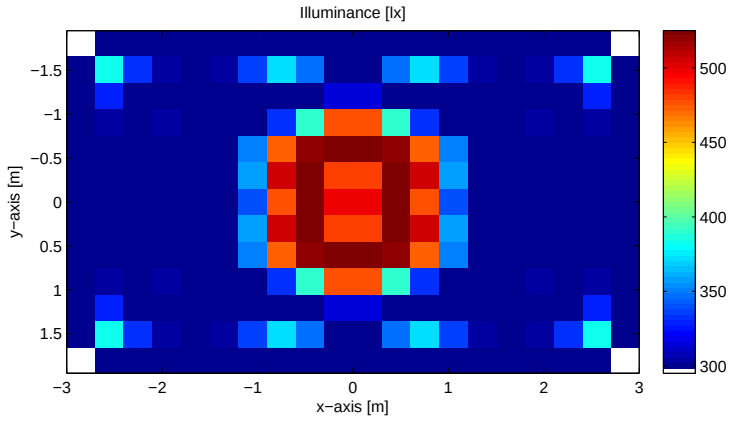

Figure 3.7: Illuminance pattern under SM-2 ($\Phi_{\frac{1}{2}} = 10.5$ degrees, C_{th}=0.05)

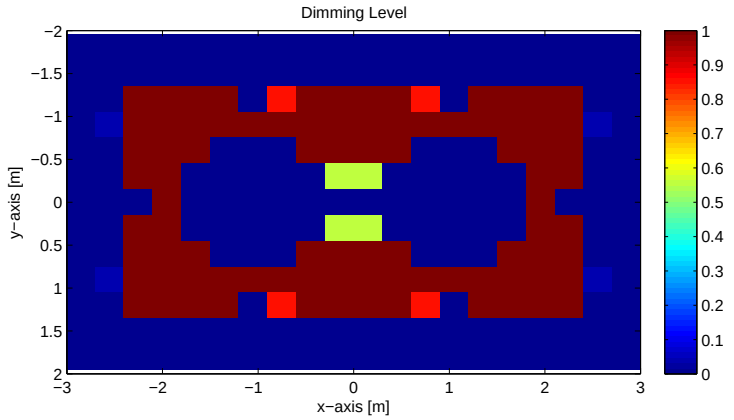

Figure 3.8: Dimming levels under SM-2 ($\Phi_{\frac{1}{2}} = 60$ degrees, C_{th}=0.05)

the occupant workspace.

$\Phi_{\frac{1}{2}}$ [degrees]	10.5	18	60
Maximum contrast (SM-1)	0.3	0.3	0.3
Maximum contrast (SM-2)	0.3	0.3	0.08
Power (SM-1) [W]	254.71	200.17	237.98
Power (SM-2) [W]	182.85	152.93	202.21
Reduction in Power [%]	28.21	23.60	15.03

Table 3.7: Performance comparison of SM-1 and SM-2 (C_{th}=0.3)

Finally, in Table 3.7, a performance comparison of SM-1 and SM-2 is shown for different $\Phi_{\frac{1}{2}}$ with $C_{th} = 0.3$. The illumination patterns, dimming levels and power savings are depicted in Figs 3.12-3.18. A looser value of 0.3 for C_{th} (i.e. lower uniformity) implies that some locations will have illumination levels as low as $0.7L_{max}$. For SM-1, those locations are principally at the borders of R_f, whereas for SM-2 these are at the

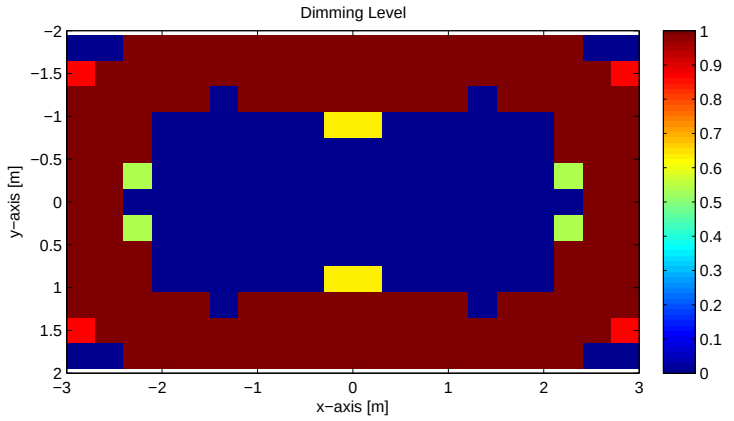

Figure 3.9: Dimming levels under SM-1 ($\Phi_{\frac{1}{2}} = 60$ degrees, C_{th}=0.05)

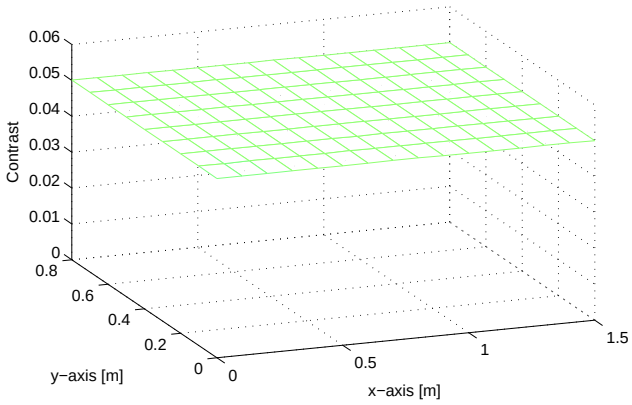

Figure 3.10: Maximum contrast for different locations of an occupant under SM-2 ($\Phi_{\frac{1}{2}} = 60$ degrees, C_{th}=0.05)

borders of R_0 (see Figs. 3.12-3.14, and cf. Figs. 3.5-3.7). It is noteworthy to mention that the power saving with $C_{th} = 0.3$ is less than that with $C_{th} = 0.05$ (see Figs. 3.18 and 3.11). This can be understood by looking at the optimized dimming levels under SM-1 and SM-2 for $C_{th} = 0.05$ and $C_{th} = 0.3$ (refer to Figs. 3.8, 3.9, 3.15 and 3.16). Under SM-1 with $C_{th} = 0.05$, a larger number of LEDs are at maximum power when compared with that of $C_{th} = 0.3$ (as shown in Figs. 3.9 and 3.16, respectively). However, under SM-2 the dimming levels for $C_{th} = 0.05$ and $C_{th} = 0.3$ are quite comparable (as shown in Figs. 3.8 and 3.15).

3.5 Conclusions

In this chapter, we formulated the design of occupancy based uniform illumination control of LED lighting systems as a constrained optimization problem. This problem can be solved using linear programming methods, and a simplex algorithm was used to obtain an optimal solution. We then compared the energy efficiency of such an LED

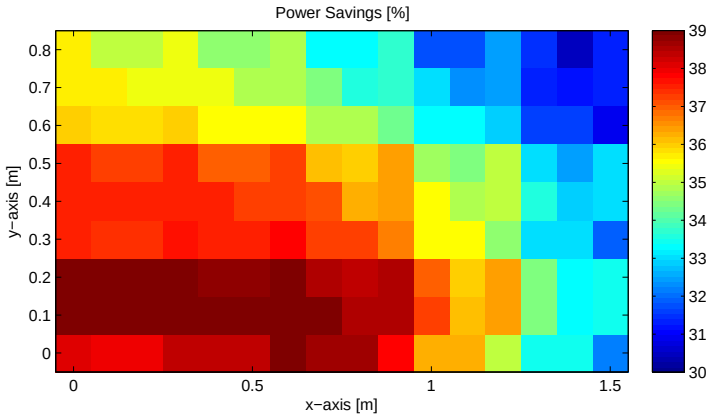

Figure 3.11: Power savings of SM-2 over SM-1 for different locations of an occupant under SM-2 ($\Phi_{\frac{1}{2}} = 60$ degrees, C_{th}=0.05)

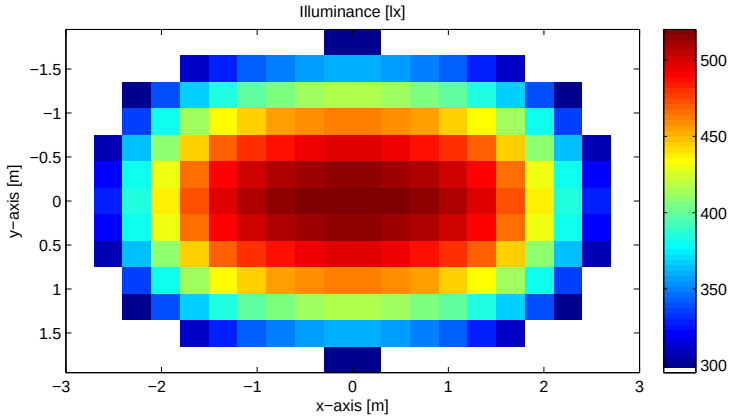

Figure 3.12: Illuminance pattern under SM-2 ($\Phi_{\frac{1}{2}} = 60$ degrees, C_{th}=0.3)

system (SM-2) with an LED system that renders uniform illumination across the entire space (SM-1). For single occupancy configurations, we showed that substantial savings are achieved with the proposed design.

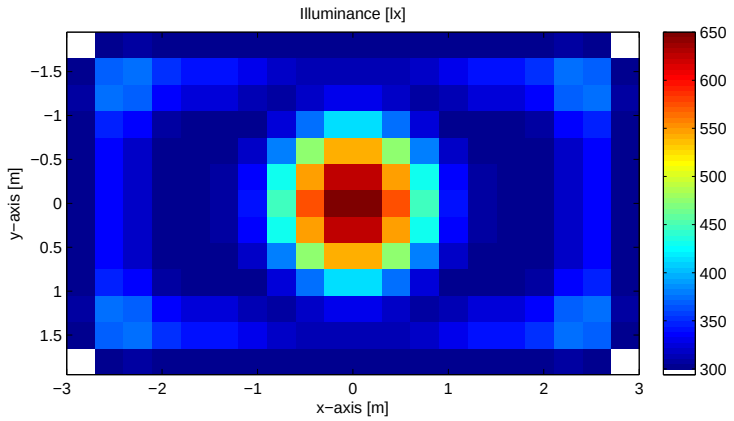

Figure 3.13: Illuminance pattern under SM-2 ($\Phi_{\frac{1}{2}} = 18$ degrees, C_{th}=0.3)

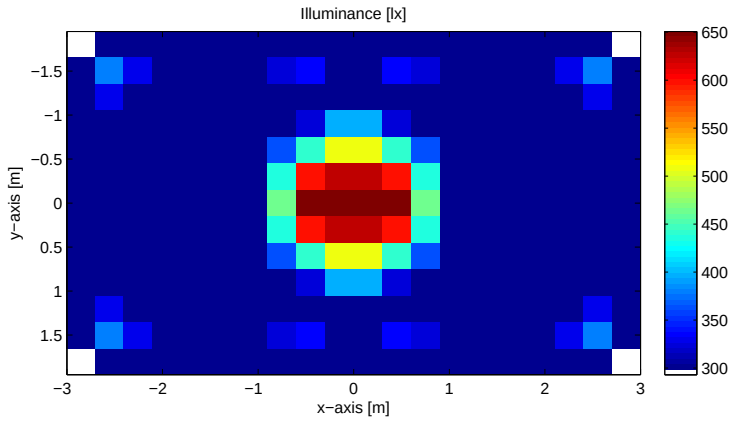

Figure 3.14: Illuminance pattern under SM-2 ($\Phi_{\frac{1}{2}} = 10.5$ degrees, C_{th}=0.3)

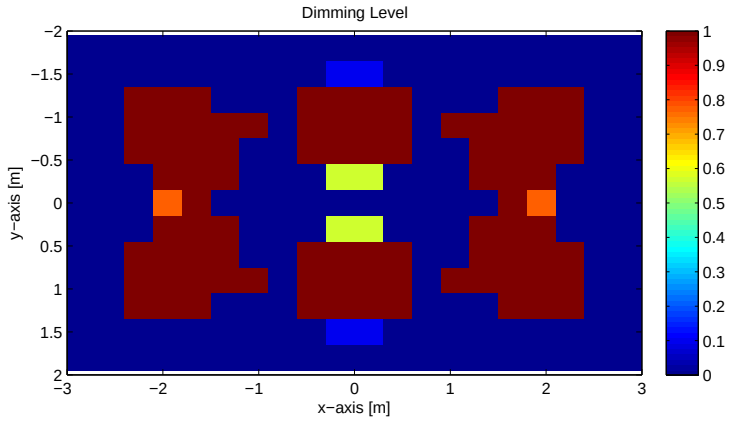

Figure 3.15: Dimming levels under SM-2 ($\Phi_{\frac{1}{2}} = 60$ degrees, C_{th}=0.3)

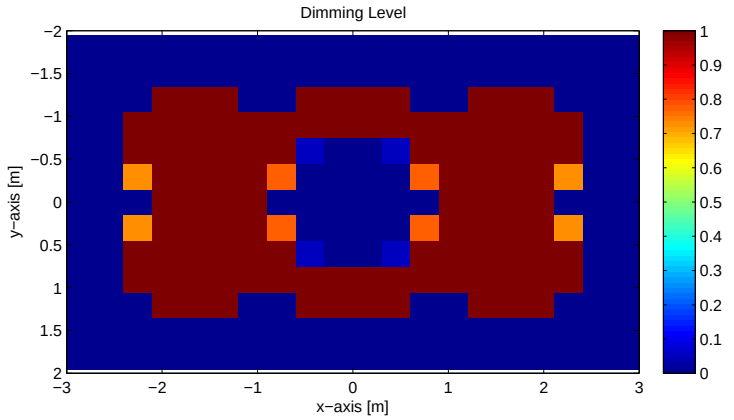

Figure 3.16: Dimming levels under SM-1 ($\Phi_{\frac{1}{2}} = 60$ degrees, C_{th}=0.3)

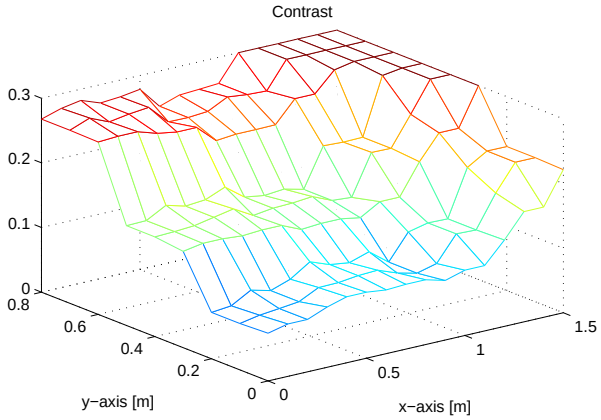

Figure 3.17: Maximum contrast for different locations of an occupant under SM-2 ($\Phi_{\frac{1}{2}} = 60$ degrees, C_{th}=0.3)

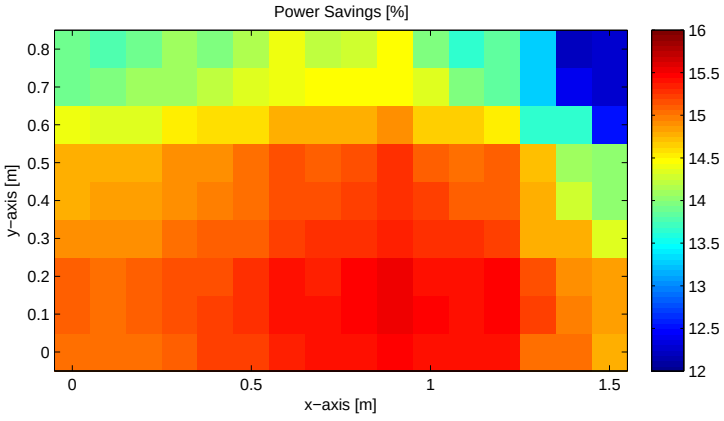

Figure 3.18: Power savings of SM-2 over SM-1 for different locations of an occupant under SM-2 ($\Phi_{\frac{1}{2}} = 60$ degrees, C_{th}=0.3)

Experimental and numerical results

4

In this Chapter, the ultrasonic sensor solution proposed in Chapter 2 is evaluated under pre-defined experiments in a test room. These results are used later as an input for the illumination control algorithm presented in Chapter 3.

4.1 Experimental results for ultrasonic sensor array solution

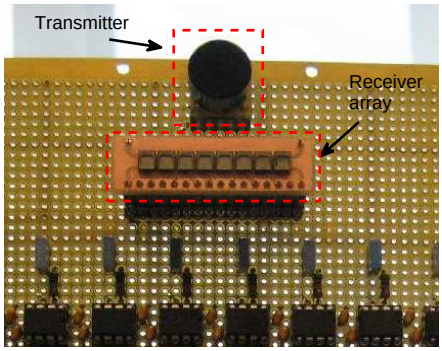

Figure 4.1: Ultrasound sensor array solution

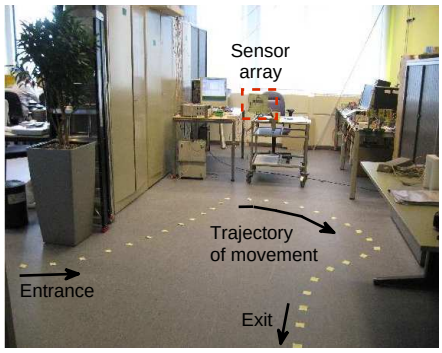

Figure 4.2: Test room and trajectory of the occupant

We evaluate the performance of the sensor array solution depicted in Fig. 4.1 in a test room shown in Fig. 4.2. The dimensions of the room are $l = 4.5$ m and $w = 3$ m.

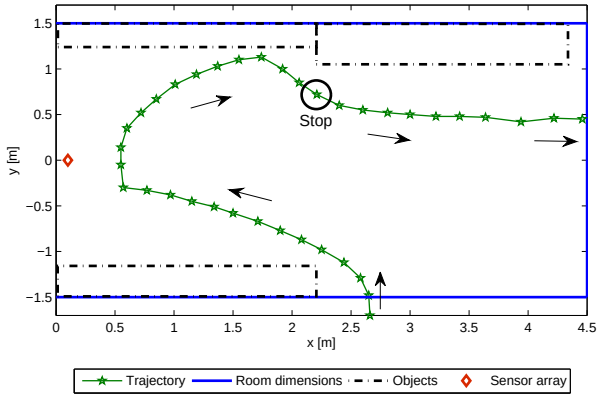

Figure 4.3: Diagram of the room and trajectory of the occupant

The sensor array is located at a height $\hat{h} = 1.2$ m. The trajectory of the occupant is depicted on the floor by a number of marked points in Figs. 4.2 and 4.3.

Parameter	Value
Model	400EP14D
f_c [kHz]	40
Bandwidth [kHz]	2
Beam angle (azimuth) [degrees]	125
Beam angle (elevation) [degrees]	65
Driving voltage [V_{pp}]	10

Table 4.1: Parameters of the transmitter

Parameter	Value
Model	SPM0404UD5
Frequency range [kHz]	10 - 65
Directivity	Omnidirectional

Table 4.2: Parameters of the receiver

The parameters of the transmitter and receiver elements are shown in Table 4.1 and 4.2. In our application the chosen transmitter and receivers allow to receive reflections from any location in the room with enough power to be processed and so we can consider them as omnidirectional.

Additionally, the design parameters of the sensor array system are shown in Table 4.3. Note that because of the MTI operation mode, we need to transmit two consecutive pulses before processing the received signal. Hence, we have a limit in the minimum updating time for the locations equal to $2 \times PRI = 64$ ms.

We consider a minimum SNR of $C_d = 3$ dB for detecting a target. The threshold

Parameter	Value
D [m]	5
ΔD [m]	0.4
ΔDoA [degrees]	2
PRI [ms]	32
T [ms]	2
M	8
Δm [mm]	4.1
f_s [kHz]	200
Γ [samples]	200
Δx [m]	0.4
Δy [m]	0.6
C_d [dB]	3
α_1	0.95
α_2	0.95
C_{th} [dB]	9
T_{th} [s]	60

Table 4.3: Design parameters of the sensor array system

C_{th} for the tracking algorithm is chosen $3C_d = 9$ dB. Hence, at least three successive samples with SNR of C_d are required for detecting an occupant, i.e. the time for localizing an occupant under these conditions is approximately 192 ms.

The values of α_1 and α_2 are chosen close to 1. The value of $\alpha_1 = 0.95$ corresponds to approximately 15 past samples to be combined for detection in the tracking algorithm, i.e. any target is tracked for at most the last 15 samples (approximately 1 s). Similarly, the factor $\alpha_2 = 0.95$ corresponds to at least 15 samples (or 1 s) for an element of the score vector $\boldsymbol{TBD}$ to decrease by half its original value.

We choose $T_{th} = 60$ s, which corresponds to the minimum time after which we can discard a location if no new measurements updates are received.

We consider the following scenario. At the beginning of the experiment, the room is empty. Later, the occupant enters through one side of the room and walks closely along the trajectory shown in Fig. 4.3. Then, the occupant stops in the location marked in Fig. 4.3. Finally, the occupant leaves through the end of the room.

The results of our experiment are shown in Fig. 4.4. Points along the trajectory in Figs. 4.4 and 4.3 are shown by stars and the estimated locations obtained from our algorithm by asterisks. As can be seen, the estimated locations closely match the real trajectory. The crosses represent locations which have been discarded as multipath using the criterion (2.20).

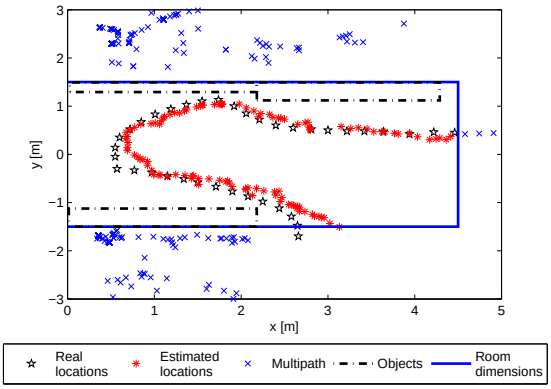

Figure 4.4: Experimental results

4.2 Results of illumination control based on localized occupancy

Finally, we integrate the ultrasonic array solution designed in Chapter 2 and the illumination control algorithm presented in Chapter 3. We evaluate the performance of the complete system by numerical simulations. We consider an LED lighting system deployed in the test room. The respectively indoor lighting parameters are shown in Table 4.4.

Parameter	Value
l [m]	4.5
w [m]	3
h [m]	2
L_{max} [lx]	500
L_{min} [lx]	300
r_0 [m]	1
C_{th}	0.05

Table 4.4: Indoor lighting parameters for testing

The parameters from Luxeon Rebel [20] are chosen for testing. Furthermore, a lens with angle $\Phi_{\frac{1}{2}} = 10.5$ degrees is used for shaping the beam. A summary of these parameters is shown in Table 4.5.

Let the separation amongst adjacent LEDs be 0.3 m. Accordingly, the parameters of LED lighting system are given in Table 4.6.

The location of the occupant obtained early in Subsection 4.1 (asterisks shown in Fig. 4.4) provides the input for the illumination control algorithm. Some practical comments on the illumination control. The control of the lighting is performed when the system detects that the occupant has stopped the movement. Otherwise, a uniform illumination across the whole space is provided.

In Fig. 4.5, the illumination pattern of the LED lighting system is shown. The

Parameter	Value
$\Phi_{\frac{1}{2}}$ [degrees]	10.5
Lambertian mode (m)	41
Maximum Illuminance (A) per LED [lx]	180
Power Consumed (P_{on}) per LED [W]	2.24

Table 4.5: Parameters of LED using lens

Parameter	Value
$\Delta x = \Delta l$ [m]	0.3
$\Delta y = \Delta w$ [m]	0.3
$N_x = N_l$	15
$N_y = N_w$	10

Table 4.6: Parameters of LED lighting system

asterisk represents the estimated location where the occupant has stopped. It can be noted that a uniform illumination at level L_{max} is provided around the location of the occupant.

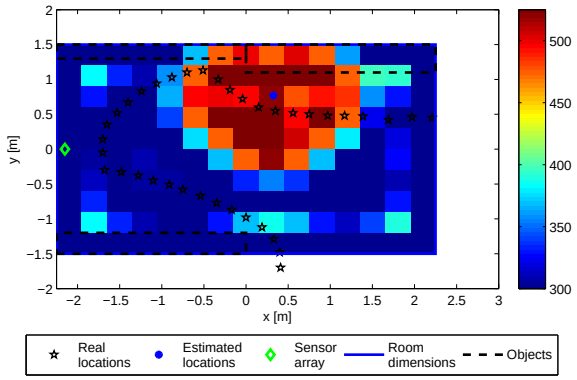

Figure 4.5: Illumination control based on estimated location of the occupant ($\Phi_{\frac{1}{2}}$=10.5 degrees, C_{th}=0.05)

5 Conclusions and future work

5.1 Conclusions

In this thesis we designed the illumination control of an LED lighting system based on occupancy information. This work comprised two major parts: design of an ultrasonic sensor array solution for localizing and tracking occupants in a room; and development of the illumination control algorithm.

The approach used for the design of the ultrasonic sensor array solution is based on range and DoA estimation techniques. The movement of the occupant in the room is modeled by a second-order Markov chain. Using this model, further occupancy information (e.g. movement trajectories) is obtained by implemented a tracking algorithm. We evaluated the system with a single occupant and showed the performance of the system in a real scenario. Furthermore, we showed that using a single array sensor system, we can obtain enhanced occupancy information (e.g. localization and movement trajectory).

The design of occupancy based uniform illumination control of LED lighting systems is formulated as a constrained optimization problem. Particularly, we shown it is a linear programming problem and used the simplex method to obtain an optimal solution. We performed a comparison of the energy efficiency of such an LED system (SM-2) with an LED system that renders uniform illumination across the entire space (SM-1). Furthermore, we showed that for single occupancy configurations, substantial savings are achieved with the proposed design.

Finally, we combined both parts and evaluated the performance of the complete system by simulations based on experimental data. We showed that the proposed localized occupancy detector provides the required accuracy for achieving the desired illumination control.

5.2 Future work

The following points are recommended as future work:

Multipath: Most of the false detected targets in an indoor environment owe to multipath. We considered a simple criterion for suppressing multipath. However, in some instances the multipath can not be suppressed because it results in feasible locations (i.e. inside the room). Thus, in those instances where the multipath can not be suppressed, we require more advanced criteria for identifying and mitigating the effects of multipath. This work can be done by training a classifier with the received data and getting statistical measurements for detecting multipath.

Array sensor configuration: The used ultrasonic array sensor allows for 2-D localization in the room. 3-D localization and tracking can be obtained by using multiple transmitter and multiple receivers with different configuration (e.g. circular array). Thus, different array configurations are subjects for further study.

Distributed illumination control: A centralized approach is used for solving the problem of illumination. Depending of the LED lighting system configuration (e.g. narrower beams) a distributed approach may be preferred. The effects in the performance and complexity need to be studied.

External light sources: The illumination control problem considers the effects of the LED lighting system but no the external light sources (e.g. sunlight). The contribution of these external sources can be quantified by using light sensors distributed along the room. The new optimization problem must include this new information and provide the best solution.

Appendix

A

A.1 Far field assumption

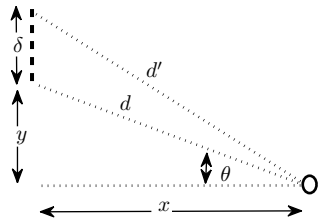

Figure A.1: Location of an object with respect to the detector

Assume the scenario in Fig. A.1, where a point target is located at a distance d and with an angle θ with respect to the sensors. The difference in distance between the first and the mth sensor is given by

$$\begin{aligned}
\Delta d &= d - d' \\
&= d - \sqrt{(y+\delta)^2 + x^2} \\
&= d - \sqrt{y^2 + 2\delta y + \delta^2 + x^2} \\
&= d - \sqrt{d^2 + 2\delta y + \delta^2} \\
&= d\left[1 - \sqrt{1 + \left(\frac{2\delta y + \delta^2}{d^2}\right)}\right] \qquad \text{(A.1)}
\end{aligned}$$

where $\delta = (m-1)\,\Delta m$.

Applying the binomial expansion to (A.1)

$$\Delta d = d\left[\frac{1}{2}\left(\frac{2\delta y + \delta^2}{d^2}\right) - \frac{1}{4}\left(\frac{2\delta y + \delta^2}{d^2}\right)^2 + ...\right].$$

By neglecting the terms of $\left(\frac{2\delta y + \delta^2}{d^2}\right)$ and similarly the term $\left(\frac{\delta}{d}\right)^2$, the expression can be reduced to

$$\begin{aligned}
\Delta d &\approx \frac{y}{d}\delta \\
&= \delta \sin(\theta).
\end{aligned}$$

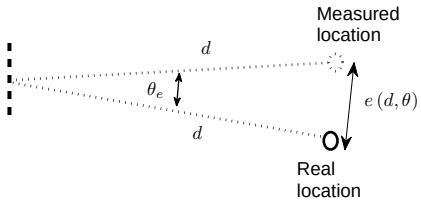

Figure A.2: Error in the measured location of a target owing to the far field approximation

However, this is only valid if those neglected terms do not contribute significantly to the result. The error between the measured and the real location (Fig. A.2) introduced by this approximation is given by

$$e\,(d,\theta) \;=\; d\sqrt{2-2\cos\left(\theta_e\,(d)\right)}$$

where

$$\begin{aligned}\theta_e\,(d) &= \tilde{\theta}\,(d)-\theta \\ &= \sin^{-1}\left(\frac{\Delta d}{\delta}\right)-\theta,\end{aligned}$$

and $\tilde{\theta}\,(d)$ and θ are the measured and the real DoA angle, respectively.

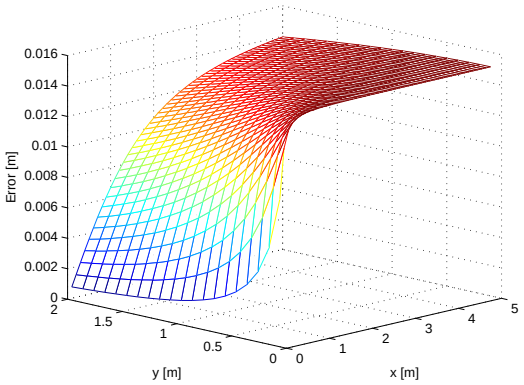

Figure A.3: Error in meters for the measured location of the occupant within the room

The error for different locations (x, y) inside the room is depicted in Fig. A.3. Because of the symmetry of the room, only the positive y coordinates are shown. As can be seen, the error is below 0.016 m, and hence negligible.

Bibliography

[1] U.S. Department of Energy, *Buildings Energy Data Book*, 2009.

[2] P. R. Boyce, J. A. Veitch, G. R. Newsham, C. C. Jones, J. Heerwagen, M. Myer and C. M. Hunter, "Occupant use of switching and dimming controls in offices", *Lighting Research and Technology*, vol. 38, no. 4, pp. 358 - 376, 2006.

[3] D. L. Loe, "Energy efficiency in lighting - considerations and possibilities", *Lighting Research and Technology*, vol. 41, no. 3, pp. 209 - 218, 2009.

[4] I. Moreno, "Creating a desired lighting pattern with an LED array", *SPIE*, paper 705811, 2008.

[5] P. Bahl and V. N. Padmanabhan, "RADAR: An In-Building RF-based User Location and Tracking System", *IEEE INFOCOM*, vol. 2, pp. 775 - 784, 2000.

[6] S. Das, C. Gleason, S. Shen, S. Goddard and L. Perez, "2-D Tracking Performance Evaluation Using the Cricket Location-Support System", *IEEE International Conference on Electro Information Technology*, pp. 1 - 6, 2005.

[7] F. van Diggelen, "Indoor GPS theory and implementation", *IEEE Position, Location and Navigation Symposium*, pp. 240-247, 2002.

[8] M. Popa, J. Ansari, J. Riihijarvi and P. Mahonen, "Combining Cricket System and Inertial Navigation for Indoor Human Tracking", *IEEE Wireless Communications and Networking Conference*, pp. 3063 - 3068, 2008.

[9] A. Ward, A. Jones and A. Hopper, "A new location technique for the active office", *IEEE Personal Communications*, vol. 4, issue 5, pp. 42 - 47, October 1997.

[10] Z. Zhen, Q. Jian, S. Song and X. Guan, "An Indoor Localization Algorithm for Lighting Control using RFID", *IEEE Energy 2030 Conference*, pp. 1 - 6, 2008.

[11] S. S. Ram, Y. Li, A. Lin and H. Ling, "Human Tracking Using Doppler Processing and Spatial Beamforming", *IEEE Radar Conference*, pp. 546 - 551, April 2007.

[12] V. Singhvi, A. Krause, C. Guestrin, J. H. Garret Jr. and H. S. Matthews, "Intelligent Light Control using Sensor Networks", *Proceedings of the 3rd International Conference on Embedded Networked Sensor Systems*, pp. 218 - 229, 2005.

[13] D. Caicedo, A. Pandharipande and G. Leus, "Occupancy based illumination control of LED lighting systems", *Lighting Research and Technology Journal*, Accepted.

[14] B. D. Carlson, "Covariance Matrix Estimation Errors and Diagonal Loading in Adaptive Arrays", *IEEE Transactions on Aerospace and Electronic Systems*, vol. 24, no. 4, pp. 397 - 401, July 1988.

[15] H. Cox, R. M. Zeskind and M. H. Owen, "Robust adaptive beamforming", *IEEE Transactions on Acoustics, Speech and Signal Processing*, vol. 35, issue 10, pp. 1365 - 1376, October 1987.

[16] Y. Boykov and D. Huttenlocher, "Adaptive Bayesian recognition in tracking rigid objects", *IEEE Conference on Computer Vision and Pattern Recognition*, vol. 2, pp. 697 - 704, 2000.

[17] L. Dong and S. C. Schwartz, "Object tracking by finite-state Markov process", *IEEE International Conference on Acoustics, Speech and Signal Processing*, vol. 1, pp. I-897 - I-900,2007.

[18] D. Musicki, "Track Score and Target Existence", *International Conference on Information Fusion*, pp. 1 - 7 , 2006.

[19] W. R. Wallace, "The use of track-before-detect in pulse-Doppler radar", *RADAR 2002*, pp. 315 - 319, October 2002.

[20] Lumileds, "LUXEON LED Radiation Patterns: Light Distribution Patterns", http://www.lumileds.com/technology/radiationpatterns.cfm.

[21] I. Moreno and C. Sun, "Modeling the radiation pattern of LEDs", *Optics Express*, vol. 16, no. 3, February 2008.

[22] H. Yang, J. W. M. Bergmans, T. C. W. Schenk, J. M. G. Linnartz and R Rietman, "Uniform Illumination Rendering Using an Array of LEDs: A Signal Processing Perspective", *IEEE Transactions on Signal Processing*, vol. 57, no. 3, March 2009.

[23] J. M. G. Linnartz, L. Feri, H. Yang, S. B. Colak and T. C. W. Schenk, "Code Division-Based Sensing on Illumination Contributions in Solid-State Lighting Systems", *IEEE Transaction on Signal Processing*, vol. 57, no. 10, October 2009.

[24] H. Yang, J. W. M. Bergmans and T. C. W. Schenk, "Illumination Sensing in LED Lighting Systems Based on Frequency-Division Multiplexing", *IEEE Transactions on Signal Processing*, vol. 57, no. 11, Nov 2009.

[25] H. Yang, T. C. W. Schenk, J. W. M. Bergmans and A. Pandharipande, "Parameter Estimation of Multiple Pulse Trains for Illumination Sensing", *IEEE International Conference on Acoustics, Speech and Signal Processing*, March 2010.

[26] P. R. Boyce, "Human Factors in Lighting", 2nd ed. New York: Taylor and Francis, 2003.

[27] Y. Gu, N. Narendran, T. Dong and H. Wu, "Spectral and luminous efficacy change of high-power LEDs under different dimming methods", *International Conference on Solid State Lighting, SPIE*, vol. 6337, 63370J, 2006.

[28] R. Otte, L. P. de Jong and A. H. M. van Roermund, "Low-Power Wireless Infrared Communications", Kluwer Academic Publishers, 1999.

[29] I. Moreno, M. Avendano-Alejo and R. I. Tzonchev, "Designing light-emitting diode arrays for uniform near-field irradiance", *Applied Optics*, vol. 45, no. 10, pp. 2265 - 2272, April 2006.

[30] S. Boyd and L. Vandenberghe, "Convex Optimization", Cambridge University Press, 2004.

[31] G. B. Dantzig, "Linear Programming and Extensions", 1st printing, Princeton University Press, 1963.

[32] D. G. Luenberger and Y. Ye, "Linear and Nonlinear Programming", 3rd edition, Springer, 2008.

[33] EN 12464-1:2002. Light and lighting. Lighting of work places. Part 1: Indoor work places. Brussels: European Committee for Standardization. 2002.

[34] Faren Srl, "FHS Lens Series", http://www.fraensrl.com/images/Fraen FLP Rebel datasheet.pdf.